UNIVERSITY OF CALIFORNIA,
IRVINE

The Comparison of the 3ω Method and the Laser Flash Thermal Measurement

THESIS

submitted in partial satisfaction of the requirements
for the degree of

MASTER OF SCIENCE

in Chemical and Biochemical Engineering

by

Zonghan Yang

Thesis Committee:
Professor Martha Mecartney, Chair
Professor Julie Schoenung
Assistant Professor Yoonjin Won

2017

TABLE OF CONTENTS

LIST OF FIGURES

LIST OF TABLES

ACKNOWLEDGMENTS

I would like to express my deep sense of gratefulness to my committee chair, Professor Martha Mecartney, who has the enthusiasm and erudition in this field. She perseveres in exploring the beauty of natural science and conveying a spirit of adventure in regard to research and scholarship, and inspiring students to find their potentials. She guided and supported us in discovering the fundamental principles yet the most mysterious puzzle in the microscopic world. I'm so pleased to join a group with such a wonderful advisor.

I also would like to thank my committee members, Professor Julie Schoenung and Professor Yoonjin Won, whose work inspired my thinking for global energy resource sustainability and thermal management in novel material design and current material innovation.

In addition, a thank you to Professor Chris Dames of University of California, Berkeley, who allowed us to learn in his group which is instrumental in understanding 3ω technique and system setup specific for ceramic material.

I thank the PhD candidates Austin Travis and Kara Philips for permission to include data from Laser flash method and simulation results in my thesis. Also, a big thank to group members Kenta Ohtaki, David Kok, Yingjie Yang and Hemanth Vijaya Kumar for helping with my research. Thanks for the financial support provided by University of California, Irvine, NSF Grant DMR-1611457.

ABSTRACT OF THE THESIS

The Comparison of the *3ω* Method and the Laser Flash Thermal Measurement

By

Zonghan Yang

Master of Science in Chemical and Biochemical Engineering

University of California, Irvine, 2017

Professor Martha Mecartney, Chair

With the global fossil fuels scarcity and environmental pollution problem becoming much severe in recent decades, novel energy resources are under evaluation. Nuclear energy is one of the most promising energy resources with advantages such as high energy density, zero carbon dioxides emission and less space. Nevertheless, safe operation and the issue of nuclear waste are problems in the nuclear industry. Multiphase ceramic material is an approach for immobilization of nuclear waste and potentially for nuclear fuel design. A composite material with 8mol% Yttria Stabilized Zirconia (8YSZ), Aluminum Oxides (Al_2O_3) and Spinel ($MgAl_2O_4$) was investigated due to potentially high thermal conductivity, good mechanical performance and radiation tolerance. OOF2 simulation work was performed based on SEM images. This thesis introduces the equipment build and standard operating procedures for a new type of thermal measurement, the *3ω* method. Thermal conductivity measurement on an 8YSZ benchmark sample as well as several 3-phase large grain (>1μm) and fine grain (~500nm) samples were performed using *3ω* method. Comparison between *3ω* and laser flash methods as well as simulation results from OOF2, MOOSE and Bruggeman modeling is discussed in this thesis.

INTRODUCTION

In the past century, fossil fuels were used intensively to reinforce the development of Industrial Civilization. Massive amounts of non-renewable resources were burned in a low efficiency and transform into electricity and heat. Up to now, the average efficiency of thermal power station is less than 40% while the rest of 60% dissipate to the ambient environment, [1] which brings up the problem with heat transfer and thermal management. As we are in the electronic times, modern science and technology are intensively pushing all the applications even smaller in dimensions and more powerful in functionalities. The problem with the miniaturizing scale is the high density of heat, which has reached to the equivalent power density of a nuclear reactor. [2] In this trend, the power density of future processors will likely have to equal a rocket nozzle in order to meet users' demands. Two approaches are oftentimes considered for managements of heat transfer in materials: 1) An efficient thermal management structure design; 2) A promising material innovation. In order to optimize the results in thermal management, improving these two aspects simultaneously can be a tough challenge for engineers.

Generally, heat exchange happens on a boundary where two materials have different physical states. [3] Some may be composed of two phase states, stationary and flowing phase, while some may exist between two stationary phases. The aims of material design not only focus on the promising heat generating material but also on the cooling side. The goal is to find some reliable materials with proper thermal conductivity both for stationary and flowing phases. An effective composite can be designed to allow faster heat dissipation for heat exchange applications or to be minimally thermally conductive for an insulation layer design. Therefore, an understanding of the correlation of thermal properties with

microscopic structure (grain boundary, porous, interfaces, etc.) of the material makes this study meaningful. Knowledge and solutions in thermal conductivity can assist engineers to avoid overheating in limited space and can improve the efficiency of heat engine. Situations like self-ignition and material degradation will probably be solved with better heat transfer solutions.

Some materials in energy industry applications such as a nuclear reactor should be configured with high-temperature durability, strong mechanical strength and radiation damage tolerance. Such properties under extreme environment are possessed by ceramic materials. Another example is in gas turbines, where coatings require material compatible with other materials, which make the demand even harsh. Ceramic material is a great candidate for many energy and engine applications. Multiphase ceramic material probably can solve such problems with a unique composition and tailored grain size. Whatever the material is, the thermal property is one of the key aspects among all the considerations.

Conventional methods thermal measurement techniques are commonly not reliable for measuring the examples we mentioned above and especially for tiny scale material with quite different thermal properties in different directions. However, a new thermal measurement design should include advantages such as time-saving and wider applicability. In this thesis, I will discuss and compare Laser Flash Analysis (LFA), Time-domain Thermoreflectance Method (TDTR), Scanning Thermal Microscopy (SThM) and the more recently developed 3ω Method for thermal property measurements in ceramic materials. Comparison between these techniques and simulation results will also be discussed.

CHAPTER 1

1.1 Motivation

From the United Nations Climate Change Conference to Intergovernmental Panel on Climate Change (IPCC), governments and scientists have been discussing the emission reduction of carbon dioxides both in developed countries and developing countries. Promises from governments to reduce carbon dioxides emission will definitely reduce the fossil fuel usage in the future, but clearly, that will require new technology development and innovation in clean energy. By 2020, the global population will approach 8 billion, [4] and how a society deals with the energy scarcity and energy waste directly relates to the national security and sustainability. The craving for energy is continuously increasing, and conventional resources are not sufficient or sensible for the whole human population. Clean energy will very likely take up a larger proportion in human society ever than before. Among all these clean energy candidates, nuclear energy attracts much attention due to its high energy density and efficiency. If the waste problem dealt with correctly, popularizing this potentially environmentally friendly method is definitely attainable. Portable energy generator will be another task for popularizing clean energy usage in daily life, requiring advanced batteries or cells act as the energy storage units for achieving this goal.

From a macro-perspective in the energy industry, we can find some great examples whose thermal properties play a decisive role, especially in extreme environment applications. In the nuclear industry, the thermal conductivity of fuel elements and other heat conducting components determine the maximum temperature a reactor can reach, which is a prominent factor in affecting reactor's performance and efficiency. Solid Oxide Fuel Cell

(SOFC), similarly has its output efficiency and endurance directly relate to the thermal conductivity of electrolytes and cladding materials. Thermal Barrier Coating is another highly advanced material system where thermal conductivity in extreme environmental applications should be optimized for gas turbines and aero-engines. Even the most common components like furnaces and boilers, and bricks and refractories are designed to possess low thermal conductivity in order to trap the heat inside instead dissipating to the ambient. Therefore, by optimizing the thermal conductivities and microstructures of the materials, we may propose some better solutions, which would be beneficial for advanced materials design.

Solid Oxide Fuel Cell (SOFC), one of applications that the material is used in an extreme environment, has a variety of advantages compared to other kinds of the fuel cells. 1. Relatively high ampere density and watt density. 2. The polarization of cathode and anode are neglectable, the main resistance is in the electrolyte. 3. Multiple clean energies available for the sources of fuel, including hydrogen, natural gas (methane) and hydrocarbons (methanol). The noble metal catalyst is unnecessary. 4. Avoided corrosion and sealing problems in acid-base and molten salt electrolyte. 5. Provided high-quality energy waste, make cogeneration possible, energy utilize ratio up to 80%. 6. Ceramics are used as electrolyte, cathode and anode, which makes the whole structure solid and avoids leakage. 7. Ceramics electrolyte requires a high-temperature operation, makes the reaction inside faster. [5] SOFC is a multipurpose energy source that not only can be used at power station for mass energy generator but also suitable as transportation media and combined cycle power generation. The first generation was the High-T SOFC whose temperature reached up to 1000℃. Later, scientists developed the Intermediate-T SOFC whose temperature was

still as high as 800℃. In order to popularize SOFC in daily life, the temperature needs to be much lower. Right now, the Low-T SOFC requires the temperature to be around 650℃. [6] Although the temperature reduced a lot compared to the first generation, it is still quite high for daily application. Even so, due to the low cost, high adaptation to fuels and high maintainability, SOFC will be one of the promising power generators in the future.

To attain its optimum state, a higher temperature in the nuclear reactor is required rather than nowadays low-temperature operation. Fast thermal transport from the fissioning fuel to the liquid surroundings in generating large volume of steam is desirable. However, a nuclear reactor cannot be operated at high temperature to reach its optimum state mainly due to the low thermal conductivity of UO_2 fuel at present. The core heats up while the exterior is still cool, and over-high temperature in the core generates fission gas bubbles and cause accumulation problems, restricting the performance of a reactor. Also, the non-fissile phase material may encounter void swelling due to irradiation. In addition, even for alkali halide model systems, such as NaCl with melting point at 1074K, are too low for nuclear system material. [7] Therefore, this high-temperature condition challenges scientists' innovation.

A developing technique called Nuclear Reprocessing is improving the nuclear waste management technology by using numbers of chemical operations that can separate uranium and plutonium from nuclear waste, [8] and supply those elements to the new nuclear fuels during processing. Even though the radiation level of nuclear waste is much lower than nuclear fuel, a material with high tolerance of irradiation is relatively preferable when using as tools during reprocessing. In addition, disposal of a complex of the nuclear

waste and heavy metal waste in coal ash are also challenging governments. [4] Formerly, the nuclear waste has several disposing options: encapsulation in glass or vitrification, crystalline ceramics or some combination of the two methods. [8] To immobilize the radioactive waste and keep it from the biosphere, consolidating the waste into a chemically stable solid form so it's easily moved and buried in a constant repository for long-time storage to avoid nuclear leakage. [9] On a microscopic perspective, radiation from nuclear fuel cause the displacements and ionization in materials which change material properties and cause tolerance issues. Any build-up of heat in the interior of nuclear waste can alter the stability of the waste and promote phase changes. So higher thermal conductivity materials are desirable for nuclear waste also.

1.2 Material of Interest

For more than fifty years, scientists in the nuclear industry tried to find a reliable way for disposing of Spent Nuclear Fuel (SNF). Japan Atomic Energy Research Institute (JAERI) did research on plutonium rock-like oxide (ROX) fuels and their burning process in light-water reactors (LWRs). The goal was to design an ROX-LWR system that can reduce the amount of plutonium after burning and potentially disposed of the spent ROX directly. [10] But for the current nuclear reactor, reprocessing dominates the recycle process in spent nuclear waste. During the reprocessing, radioactive residual probably damages the supporting materials. Therefore, to assist the process and avoid decay in material, scientists tried to find a material with better tolerance under radiation. Besides, the material should have higher thermal conductivity and mechanical strength for supporting the radioactive

nuclear waste safely. What material has been used in nuclear recycle system and immobilization can also be a candidate in nuclear fuel design.

Recent research in this area mostly focuses on the oxide ceramic materials like UO_2, ZrO_2, MgO and $MgAl_2O_4$ due to their great radiation stability. The ROX fuels mentioned previously is a multiphase mineral-like mixture with a very large grain size composed of YSZ, $MgAl_2O_4$ and Al_2O_3.[10] Al_2O_3 and $MgAl_2O_4$ have relatively high thermal conductivity than ZrO_2, therefore, properly mixing these materials will get the multiphase material with improved performance by utilizing the advantages of different material. But normally the limit number of phases is about four because of the high probability to form new phases with the more components introduced, thus reducing thermal conductivity. Thermal conductivity can also be affected by increasing amounts of pores due to different sintering, making the mechanical strength lower. Pores are easily formed at grain boundaries, Fig. 1.1 shows the amount of grain boundaries in 4-phase composite is distinctively larger than 3-phase composite.

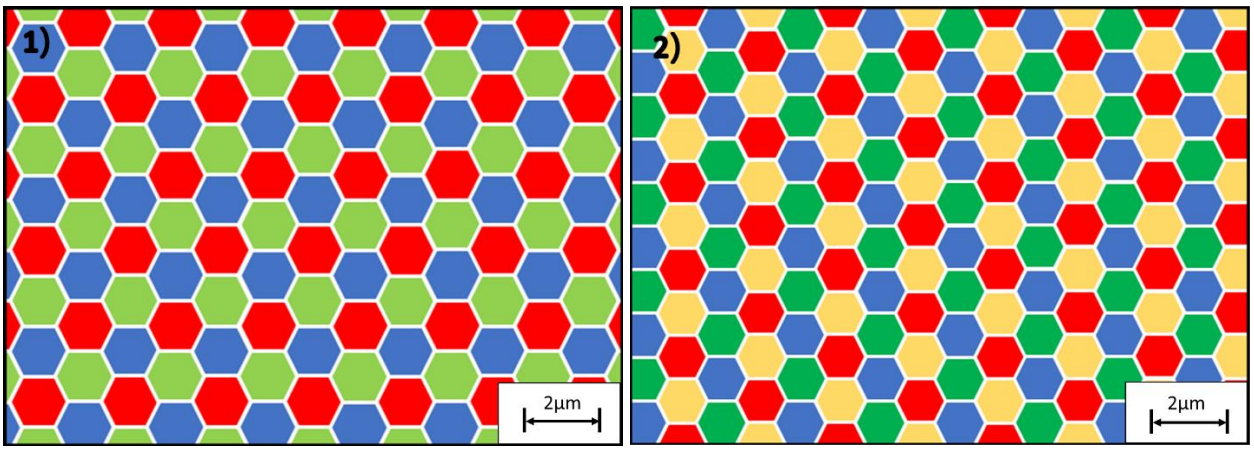

Fig. 1.1 Ideal Microstructure in 1) 3-Phase and 2) 4-Phase Composite

Aluminum Oxide (Al_2O_3) is a common ceramic material uses widely in industry. Molar mass is 101.96 $g \cdot mol^{-1}$. Density is around 4 $g \cdot cm^{-3}$ based on the different form of the material. [11] Usually, it is white solid or powder with no odor. It can be used as the raw material for making aluminum metal and it is also used widely in abrasive grinding machine and cutting tools due to its hardness, which is higher than most ceramic materials. Commonly, for refractory material in a furnace and thermal barrier coating, Al_2O_3 possess superiority due to its high melting point. Al_2O_3 is not an electric conductive material (band gap is 7eV [12]) but with a relatively high thermal conductivity at room temperature, around 30 $W \cdot m^{-1} \cdot K^{-1}$. [11] Because of its great hardness performance, high melting point and relatively high thermal conductivity, this material fit in some extreme environment applications such as a nuclear reactor, well drilling and mining. Al_2O_3 is one of the typical metal oxides used in nuclear applications owning to high damage resistance under irradiation. Therefore, Al_2O_3 is one of the promising candidates in the nuclear waste study. Fig. 1.2 shows Al_2O_3 crystal structure. [13]

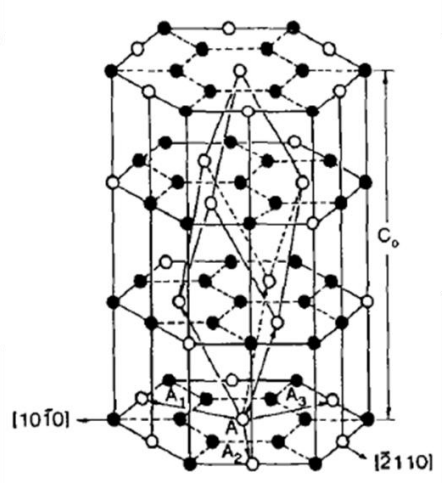

Fig. 1.2 Alumina (Al_2O_3) Crystal Structure [14]

8mol% Yttria Stabilized Zirconia (8YSZ) is another ceramic material. In general, pure zirconia goes through a series of phase transformation when heating up the material. When the temperature reaches to 1173℃, monoclinic zirconia transforms to tetragonal. If temperature continuously increases, the cubic structure appears at 2690℃. Above that, zirconia crystal will melt when the temperature reaches to its melting point. When cooling down sintered zirconia, the tetragonal to monoclinic phase transformations cause cracking. However, Zirconia shows up good radiation damage resistance when it is stabilized. [14, 15] If Zr^{4+} is substituted by large radius ions such as Y^{3+}, a more stable zirconia forms over a wide range of temperatures, such as 8mol% Yttria Fully Stabilized Zirconia (8YSZ). In our study, we use cubic 8YSZ as a surrogate for UO_2 as these materials have the fluorite structure and similarly low thermal conductivity. YSZ also plays the role of electrolyte in SOFC because of its oxygen ion-conducting property, high thermal shock and corrosion resistance. [14] Therefore, not only the physical-chemical stable properties are useful in refractory applications, but also the great irradiation stability when in contact with actinides makes YSZ an ideal candidate for inert matrix fuels in the nuclear industry. [16] Due to the similar properties of 8YSZ and UO_2, it can be used as surrogate for simulating the mechanical and thermal property of the multiphase ceramic. Fig. 1.13 shows YSZ crystal structure.

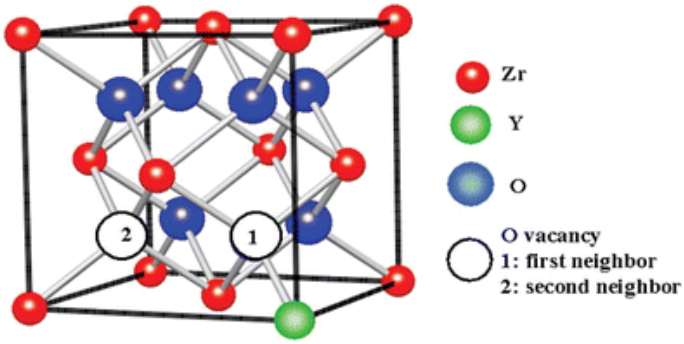

Fig. 1.3 Crystal Structure of Yttria Stabilized Zirconia (YSZ) [17]

$MgAl_2O_4$ (Spinel) is an excellent oxide refractory structural material. The general formula of a Spinel is XY_2O_4 while Magnesium Aluminate Spinel ($MgAl_2O_4$) is one type of spinel. Early times, spinel was used as gemstones for decoration because of its attractive color. Later, scientists discovered and utilized its unique chemical, physical and thermal properties in different technical applications. Because of its high melting point, 2135°C, [18] and high damage resistance to a wide range of acids and alkalis, it appears frequently in high-temperature devices such as the lining of steel-making furnace, burning zone of cement kilns, sidewall and bottom of the steel ladles. [19] Most materials under radiation will show some defect aggregations such as voids and loops. On the contrary, spinel is capable of annihilating this problem by interstitial-vacancy recombination. [20, 21] Research on Spinel show better radiation resistance than other ceramic material like alumina or magnesia. [22] For the rest of paper, the term Spinel will be used as representative of $MgAl_2O_4$. Fig. 1.4 shows Spinel crystal structure. [13]

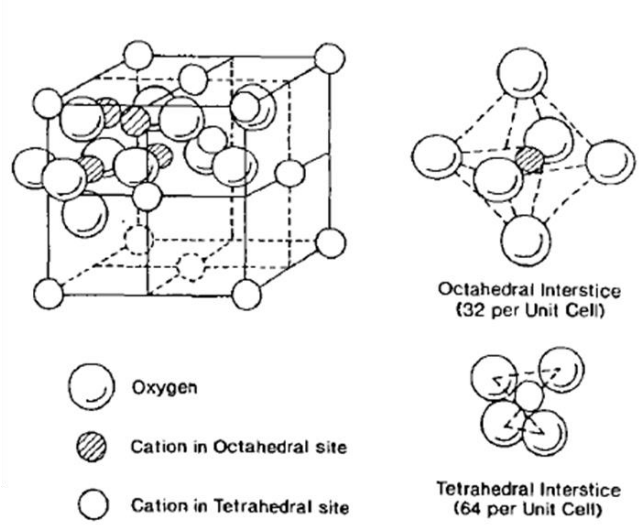

Fig. 1.4 Crystal Structure of Spinel ($MgAl_2O_4$) [13]

Fig. 1.5 shows three ceramic materials of interest for their thermal conductivity versus temperature. It should be noted other ceramic materials such as perovskites ($CaTiO_3$) and pyrochlore ($Gd_2Ti_2O_7$ and $Gd_2Zr_2O_7$) are also candidates for actinide immobilization in nuclear waste. [22] Alumina (Al_2O_3), Yttria Stabilized Zirconia (YSZ) and Spinel ($MgAl_2O_4$), are the most common low price ceramic materials in the industry, which becomes a great benefit in studying them.

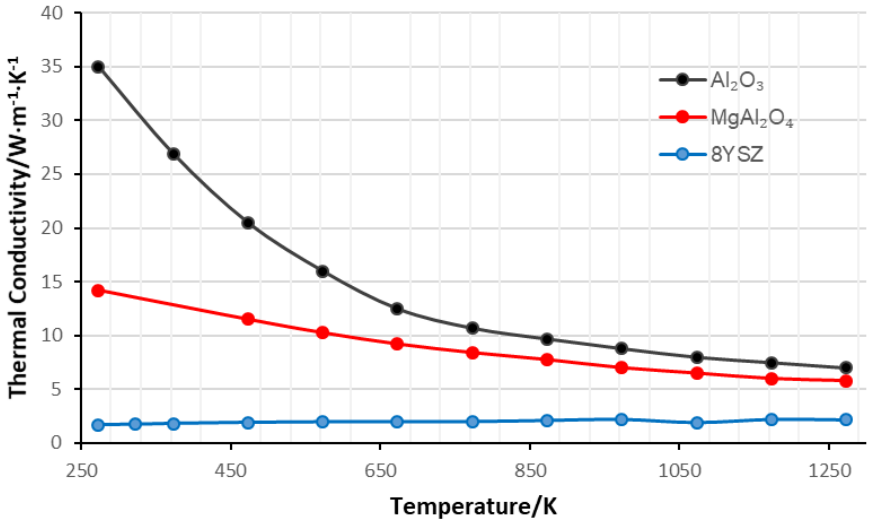

Fig. 1.5 Thermal Conductivity for Each Single Phase from Literature (Al_2O_3, [11] $MgAl_2O_4$ [19] and 8YSZ [23])

Table 1.1 Ceramic Materials Property

	Density [g/cm^3]	Melting Temperature [°C]	Thermal Expansion Coefficient [($°C^{-1}$)x10^{-6}]	Elastic Modulus (GPa)	Thermal Conductivity (W/m•K)	Poisson's Ratio
Al_2O_3	3.97[11]	2323[26]	7.2-8.8[24]	366[24]	33[11]	0.26[26]
$MgAl_2O_4$	3.6[18]	2135[18]	8.8[28]	241[24]	12.4[19]	0.268[24]
8YSZ	6.0[25]	~2700[26]	10.5 [29]	220[27]	1.7~2.1[23]	0.22[26]

1.3 A Brief Review of Ceramic Material in the Nuclear Industry

In order to improve the performance of the nuclear reactor, Department of Energy (DOE) collected some innovative ways for the fast reactor fuels. [30] Designs from several national labs and research results in numbers of universities proposed some probable ways for dealing the problems. The top three ranked methods are mainly about using advanced fuel for the nuclear reactor. Some additional methods described as potential ways by using the advanced material for enhancing the performance of the nuclear reactor.

One proposal focused on studying high burn-up ceramic composite inert matrix nuclear fuels to enhance the thermal conductivity of oxide fuels to optimize nuclear reactor tolerance and durability. [30] Some problems like swelling, thermal and radiation-induced materials creeping and cracking was demonstrated to be solved by using multiphase ceramic materials. Non-fissile phases play a crucial role in this material because it can control fission product accumulation and arrest undesirable microstructural evolutions. Some oxides, for example, MgO and Al_2O_3, are susceptible to void swelling, so a mixture of these two oxides, $MgAl_2O_4$, has a better ability for reducing the void swelling problem. Reasons including: 1) Large critical size of dislocation loop nucleus caused by complex chemistry; 2) Complex structure generates constraints can prevent the dislocation loops from un-faulting; 3) The cation sublattices in spinel very likely be disordered by high-fluence neutron irradiation. [20] As for other oxide materials, some of them possess these abilities for reducing microstructural evolution.

Valdez et al. [31] used 10MeV Au^{3+} ion irradiation on 90-mole% MgO and 10-mole% HfO_2 ceramic-ceramic (CER-CER) composite to evaluate the irradiation result on this material.

They observed order-to-disorder (O-D) transformation (rhombohedral-to-cubic) in the $Mg_2Hf_5O_{12}$ under the highest fluence of 5×10^{20} Au/m^2 during the investigation. The MgO matrix and $Mg_2Hf_5O_{12}$ second phase were not changing their phase state, still remaining crystalline. *Men et al.* [32] investigated the radiation damage in the four-phase ceramic composite with 3 mol% YSZ, Al_2O_3, $MgAl_2O_4$ and $LaPO_4$ (See Fig. 1.6a). The experiment was performed under 10MeV Au ion at 500 ℃and 92 MeV Xe ion at 800 ℃. Al_2O_3, 3YSZ and $MgAl_2O_4$ phases were observed to have high amorphization resistance and remain consistent under irradiation with both Au and Xe ions. However, a phase transformation happened in 3YSZ due to the irradiation by Au and Xe. In addition, $LaPO_4$ monazite phase melts and dewets other phases (See Fig. 1.6b) then recrystallized under Au irradiation, on the contrary, no phase changes were observed under Xe irradiation.

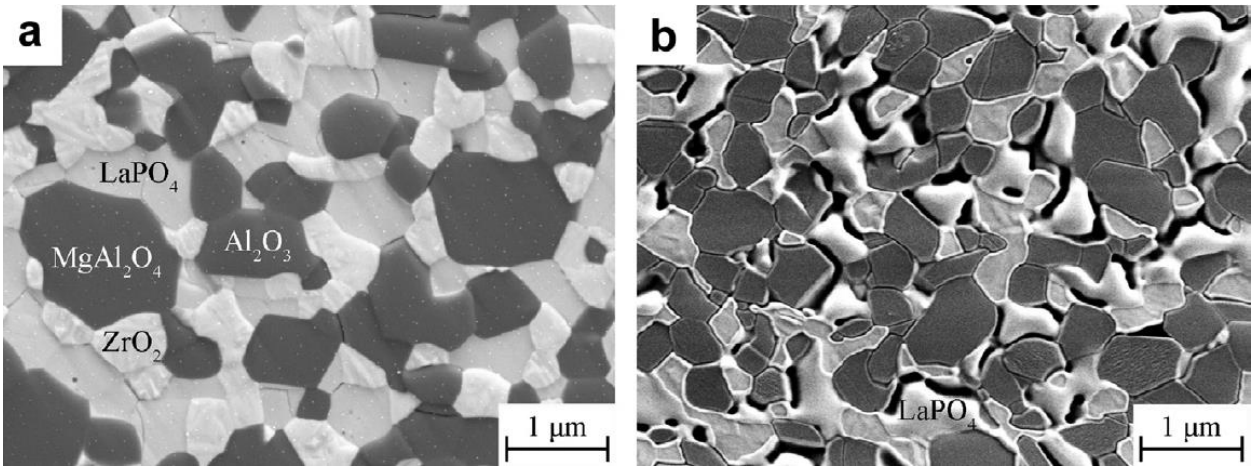

Fig. 1.6 SEM Image on The Four-phase Ceramic Composite. a) Before Au ion irradiation; b) $LaPO_4$ appeared to melt during irradiation and dewet to minimize the surface of monazite [32].

Yamashita et al. [10] performed irradiation test on ROX using YSZ mixing with UO_2, Spinel and Al_2O_3. YSZ showed perfect irradiation tolerance with a very low fission gas release (FGR), negligible void swelling and almost zero restructuring. In addition, they compared

particle dispersed fuels (YSZ inclusion size: 250μm) and mechanically powder mixture fuels (YSZ inclusion size: 10-50μm) in swelling and FGR, the former one showed lower void swelling but higher FGR than the latter one. A composite fuel composed of 20mol% YSZ, 37.1mol% UO_2 and 42.9mol% $MgAl_2O_4$, YSZ inclusion size: 10-50μm, was named SH fuel. When the temperature was over 1700K, they observed Al_2O_3 formation in samples initially without Al_2O_3, so they conjectured that $MgAl_2O_4$ decomposed under that temperature and MgO vapor might be the driving force of the central hole formation. MgO was observed on the inner surface of the cladding, phase identified by Electron Probe Micro-Analyzer (See Fig. 1.7). The thermal expansion difference in YSZ and spinel may be the reason for cracking, therefore, further improvement will be focusing on sintering condition and tailoring density and the gap width between YSZ and spinel.

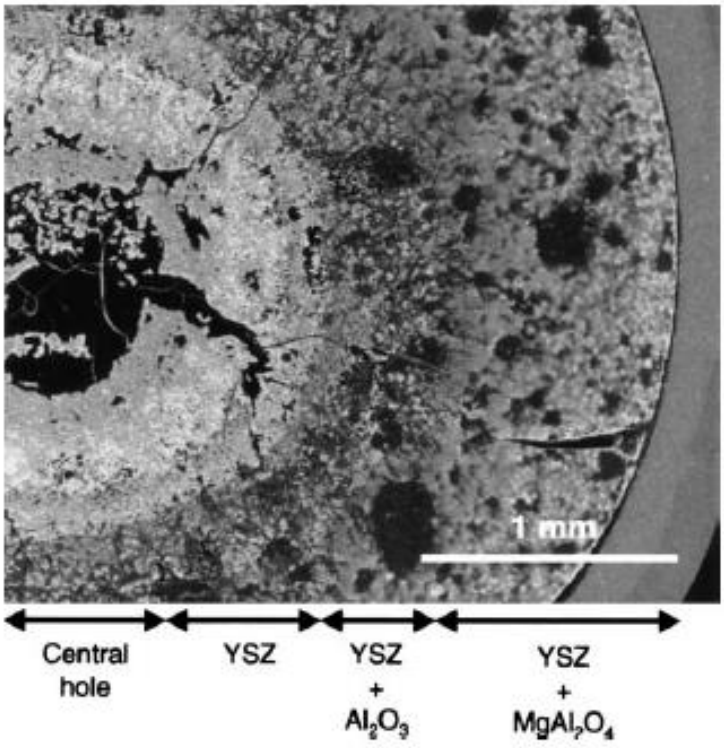

Fig. 1.7 SEM Image of Irradiation on SH Fuel (20mol% YSZ, 37.1mol% UO_2 and 42.9mol% $MgAl_2O_4$, YSZ inclusion size: 10-50μm) [10]

1.4 Thermal Transfer in Ceramic Material

Former research has proposed plenty of materials that potentially could be used in inert matrix nuclear fuel design and nuclear waste host design. In addition, various of papers have evaluated individual material properties like irradiation resistance property, mechanical property and thermal property, etc. Some materials' mechanical property failure is caused by thermal property changes with temperature rise. Sometimes, phase or structural changes in materials will cause thermal property reduction and likely lead to a disaster in the industry, which again, proves the significance of this study.

Thermal shock is a serious challenge in most of the ceramic materials when it undergoes rapid temperature change, mostly upon cooling. This susceptibility to temperature changes is an undesired property, especially in an extreme environmental application like a nuclear reactor. Eventually, a failure in ceramic material will cause a deteriorated situation and a large number of economic loss. Some researchers have observed cracking, [10] swelling and decomposition phenomena in nuclear fuels.

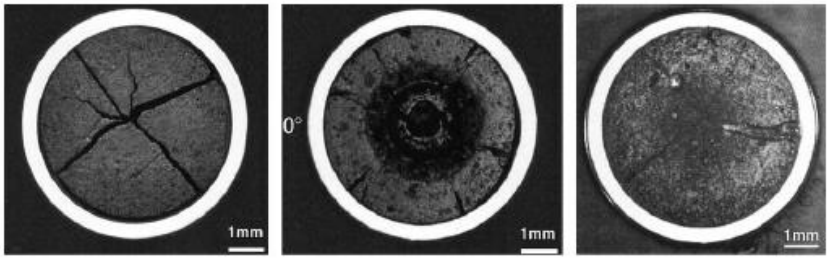

Fig. 1.8 Cross-section Image on Different Component Materials after Irradiation [12]

In conclusion, a comprehensive study should be performed in this field, including thermal, mechanical and chemical properties of ceramic materials. My study mainly focuses on thermal property of ceramic multiphase material.

The response of a material when subjected to a heat flux q gives the thermal conductivity k [33]. Based on Fourier's law:

$$q = -k\nabla T \quad (1)$$

Heat flux equals to thermal conductivity times temperature gradient. Thus, heat transfer direction is perpendicular to isotherm and point at low-temperature side. Fourier's law simply reveals that thermal conductivity is the connection between heat flux and temperature gradient.

In ceramic material, energy is absorbed in the form of heat and transfer to the low-temperature side. During the heat transfer process, crystal structure may change, the dimension of material may also change due to thermal expansion and eventually when the temperature reaches a certain point, the material melts. Oftentimes, we take thermal conductivity, thermal expansion and heat capacity as baselines measurements for the thermal properties of a material.

When considering heat transfer, normally we can simplify different cases into some types of scenario. In solid state or some high viscosity materials, heat transfer mainly attributes to thermal conduction. In liquid, gas or some low viscosity phases, thermal convection and radiation dominate the situation. [3] For interphase heat transfer, we need to consider both heat transfer types. In most solid-state materials, electrons and phonons are two dominant particles that play the role as carriers of heat. [33] For most electrically conductive material, electrons are responsible for the heat conduction while for dielectric materials, phonons are dominant. Phonon is not like electron because it has no mass and it is only a normal mode of lattice vibration in crystals. In solid state physics theory, an atom or a molecule in

crystalline state material vibrates around its equilibrium position. [34] Each atom or molecule does not vibrate independently, it usually has interaction forces with particles around it. Simply we can treat the interaction between atoms as an elastic force. Phonon is a simplified quantum model for lattice vibration in a crystal structure.

Lattice vibration conductivity is generally smaller than electron conductivity. [33,34] Phonon is not as effective as electron mainly because scattering is likely occurred by lattice imperfections. Specifically, due to the scarcity of a large number of free electrons in ceramic materials, phonons take over the role for heat conduction. Since the lattice vibration dominate, ceramic materials intrinsically possess low thermal conductivity. High-temperature situation intensifies the collision between phonons, which lead to an enhanced phonon scattering as well. Therefore, a phonon mean free path at high temperature tends to be shorter than the distance at room temperature. Other factors such as impurity, porosity and grain boundary will further reduce thermal conductivity of ceramic materials. A combined effect by these factors make ceramic materials into a dielectric material with low thermal conductivity.

1.5 Factors in Thermal Transfer

Applications which require the material with high thermal conductivity, need to avoid pores inside the material and reduce any defect such as the number of point defects or grain boundaries that lead to low thermal conductivity adulteration. [24] However, sometimes doped material will have even higher thermal conductivity mainly because those doping phases have high thermal conductivity and promote overall thermal conductivity. Our research primarily focuses on nuclear industry material, where we want

to have high resistance to irradiation, high thermal conductivity, high mechanical strength and great chemical stability tolerance. All factors are interrelated and some factors may impact on thermal property. From a microscopic perspective, several complementary factors potentially affect thermal conductivity of ceramic: [24,33]

1. Phonon conductive versus electron conductive: electron conductivity is higher than phonon conductivity. Thus, any ceramic material with electric conductive property would be conducive for higher thermal conductivity.
2. Lattice imperfection (Point defects):
    a) Self-interstitial Atom: Two close atoms share a lattice site, which becomes the center of this diatom system.
    b) Substitute Impurity Atom: A different element atom substitutes the position where a lattice atom should be.
    c) Interstitial Impurity Atom: Similarly, a different element atom but usually smaller than the lattice atoms is intercalated in the lattice and cause the defect in the material.
    d) Vacancy: Simply an atom disappears and causes a vacancy in the matrix. Such vacancy not only blocks vibration wave transfer but also make the lattice inconsistent.

    Point defects generally impact on the surrounding atoms vibration and disturb the uniformity of lattice. Those effects become the impedance in heat transfer.

Defects exist both on the atomic scale and larger scale, some even can be observed by an optical microscope. Defects on a larger scale consist of:

1. Impurity: The doped element in the lattice disrupts normal lattice arrangement. When temperature rises, as the mean free path of all the atoms approachs to the dimension of a unit cell, the whole material thermal conductivity decreases.
2. Porosity: Similar to a vacancy in lattice site, the only difference is that pores are a collection of vacancies in three dimensions. The thermal conductivity of air is $0.026 W \cdot m^{-1} \cdot K^{-1}$, much smaller than the thermal conductivity of the ceramic material. Therefore, a significant thermal conductivity drops when there is a great proportion of porosity in a material, since pores often have trapped air inside.
3. Grain Size: The mean free path of a phonon is much larger than an electron. At room temperature, a phonon's mean free path is significantly smaller than grain size for most large grained ceramics. So, in that case, phonon scattering at grain boundaries does not play an important role in reducing thermal conductivity for the most room temperature application.
4. Dislocation: This defect is an irregular crystal structure exists in the lattice. A core exists on the dislocation situation, where density and structure changed. Strain field changes in a wide range around a core (See Fig. 1.9). All these situations can cause phonon scattering.

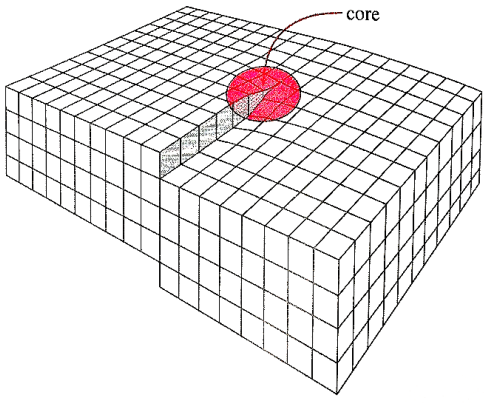

Fig. 1.9 Dislocation Defect in Lattice [24]

Those defects or imperfections lead to a lower thermal conductivity of the material. Some can be eliminated by using advanced process and high purity raw material, some problems may exist constantly in the material no matter how current technique be improved. Another intrinsic factor is the Thermal Boundary Resistance (TBR), which parasitically exists between two grains. [35] Three imperfections naturally exist in the material as the form of thermal boundary resistance: Incomplete contact, near-interfacial disorder and acoustic impedance mismatch.

1.6 Thermal Boundary Resistance

Heat transfer at interfaces is highlighted intensively in modern technology, due to the miniaturization magnifying the problem in microprocessors and integrated circuit. At solid/solid interface region, a temperature discontinuity is observed. At a grain boundary, the temperature tends to 'shift' rather than be continuous even though the average thermal property of two solid materials are the same. But at a grain boundary there are two different crystallographic orientations in each grain. If we take a close look at the interface at steady-state, the temperature distribution is shown in Fig. 1.10.

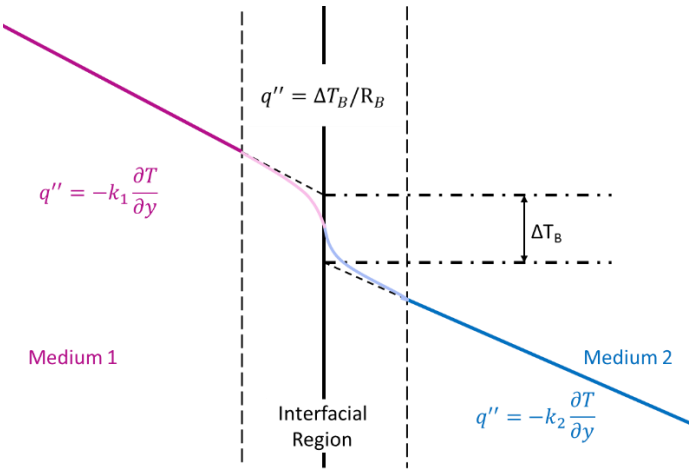

Fig. 1.10 Steady-state Temperature Distribution [36]

From the extrapolations of two temperature profile, a ΔT_B exists at interfacial region, which becomes the discontinuity at interfaces. Factors such as additional layer, interfacial roughness and species difference may become the reason for carriers scattering near boundary. *Monachon et al.* [35] in the thermal boundary conductance review paper showed that a carrier with characteristic parameters has probability α_{12} (See Fig. 1.11) to be scattered at interface. Integration over all carriers can get a summarized irradiance with a weighted average transmission coefficient. The macroscopic image simplifies the irradiance to thermal boundary resistance, which is easier for analyzing.

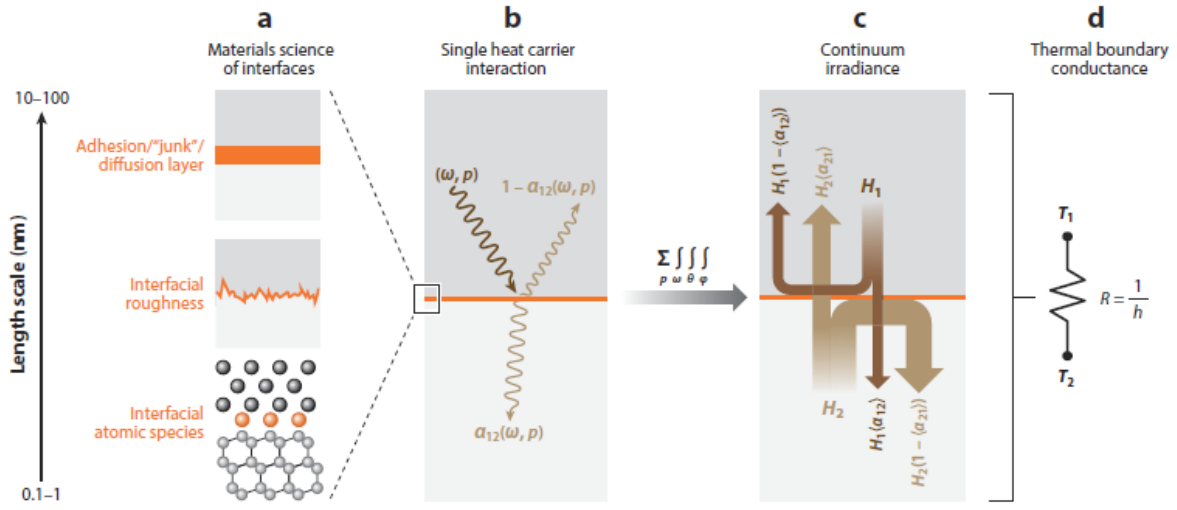

Fig. 1.11 Scattering at Interfaces Influencing Factors and Relations [35]

Incomplete contact is an intrinsic problem regardless of the smoothness of the surface. The boundary resistance $R_{B,C}$ due to incomplete contact relates to the contact fraction f_c, average conductivity k_{avg}, contact radius r_c, contact density n_c. The expression is: [36]

$$R_{B,C} \sim \frac{(1-\sqrt{fc})^{1.5}}{2\, k_{avg}\, r_c\, n_c} \tag{2}$$

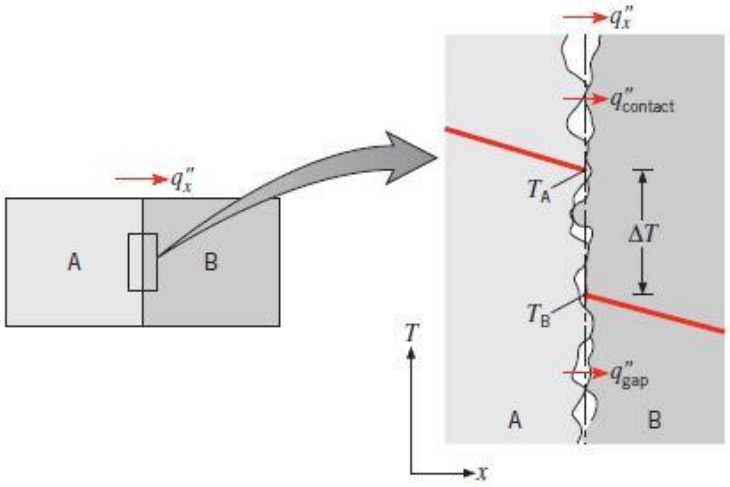

Fig. 1.12 Incomplete Contact Resistance [37]

Near interface disorder means the defective layer near the surface due to the different thermal conductivities on that disordered interface, so the thermal boundary resistance relates to the defective layer thickness Δx_d and defective thermal conductivity k_d and pure thermal conductivity k_1. The expression is proportional to the layer thickness: [36]

$$R_{B,D} \sim \frac{\Delta x_d}{k_d} - \frac{\Delta x_d}{k_1} \tag{3}$$

Acoustic Impedance Mismatch is another imperfect factor. The resistance of this mismatch relates to the heat capacity C_1 and C_2 and group velocity v_1 and v_2: [36]

$$R_{B,AMM} \sim \frac{1}{C_1\ v_1} + \frac{1}{C_2\ v_2} \tag{4}$$

Other than the imperfect defects at interfaces, thermal resistance exists at grain boundaries and interfaces is called interfacial thermal resistance, or *Kapitza* resistance. [38] This differs from contact resistance, which exists even in the theoretical perfect contact material. Although we can control the amount of boundaries or boundary type by tailoring grain size, synthesizing single-phase or multiphase materials respectively, we cannot ignore boundary

effect in material. Due to the variable electronic and vibrational characteristics in different materials, phonons and electrons are scattered when they attempt to traverse the interface.

Early scientists observed temperature drop between metal and helium interface much larger than they expected, [38] they discovered that interfacial resistance played an important role in heat transfer between interfaces. Later, *Kapitza* resistance expanded the definition to metal and dielectric materials and two dielectric materials (intimate contact condition). When a phonon travels to the interface, both reflection and refraction occur at the boundary.

Two types of the model are utilized widely for simulation of the conductance at the boundary, Acoustic Mismatch Model (AMM) and Diffuse Mismatch Model (DMM). [39] The difference is that AMM assumes that at the boundary the surface is geometrically perfect, while for DMM mostly focuses on the interface with characteristic roughness, therefore, DMM is more accurate using diffusing to explain scattering at the interface. A theoretical standard to determine the resistance at the interface is the overlap of phonon state on both sides of material A and B. When phonon transfer from high phonon density side to low-density side, due to the acceptable phonon density difference, less energy transfers to the lower side. Such that phonon scattered effect become resistance at the boundary. When phonon transfer from low phonon density material to high phonon material, the lower side cannot give as many phonons as the higher side can accept, where a thermal boundary resistance appears.

Even though these two models are based on different assumptions, both of them still follow some fundamental equations. The energies are not the same when carriers transfer in

different directions, mainly because of the density of phonon distinct on each side. When phonon transfer from A to B, the flux of energy is: [35,39,40]

$$\mathrm{Q_{A,B}} = \sum_k \mathrm{n}(k, \mathrm{T_A}) E(k) \alpha(k, T_A, T_B) \tag{5}$$

n: The number of phonon at a given wavevector and momentum;

E: Phonon energy

α: The probability of transmission across the interface.

k: Number of phonons.

$\mathrm{T_A}$ & $\mathrm{T_B}$: Temperature in A and B side, respectively.

Since the flux of energy is different from each direction, a net energy flux is expressed like:

$$\mathrm{Q_{net}} = \mathrm{Q_{A,B}} - \mathrm{Q_{B,A}} \tag{6}$$

The flux of energy depends on the temperature gradient, which means there is a temperature difference on each side. Based on the analog thermal circuit analysis, we have the equation to determine thermal interface resistance:

$$\mathrm{R}_{th} = \frac{\Delta T}{Q_{net}/A} \tag{7}$$

R_{th}: Thermal interfacial resistance.

A: Total interface area.

Q_{net}: Net energy flux across the interface.

ΔT: Temperature difference on each side of the grain boundary.

We can calculate the interfacial resistance using the equation above. However, it is hard to get an accurate result because we cannot make sure that material perfectly contacts and

some defect and impurity always exist in the material. By simulation, we can theoretically calculate interfacial thermal resistance. *Wang et al.* [41] did computational work on interfacial thermal resistance by using DMM. Their interfacial thermal resistance equation based on previous study is expressed as the following:

$$R_{\text{int}} = \frac{1}{\sigma_K} = \frac{1}{2}\sum_{i,j}\frac{\partial}{\partial T}\int_0^{\pi/2}\int_0^{\omega_i^{max}} \alpha_{i,j}(\theta,\omega,j)g_{i,j}(\omega)n(\omega,T)\hbar\omega v_{i,j}\cos\theta\sin\theta d\theta d\omega \qquad (8)$$

R_{int}: Interfacial thermal resistance;

σ_K: Interfacial thermal conductance

$\alpha_{i,j}$: The probability of transmission across the interface from *i* in mode *j*.

θ: Phonon incident angle;

ω & ω_i^{max}: Phonon angular frequency and maximum value in side *i*, respectively.

$g_{i,j}$: Density of phonon state of mode *j* in side *i*.

$n(\omega,T)$: Bose occupation distribution function, $n(\omega,T) = \frac{1}{e^{\hbar\omega/k_BT}-1}$, where k_B is Boltzmann constant, T is temperature.

T: Temperature in *i* side.

$\hbar$: Planck's constant

$v_{i,j}$: Phonon sound velocity of mode *j* in side *i*.

They used 50 kinds of solid materials to form totally 1250 kinds of interface. Some of the interfaces' properties could be found in literature like sound velocity in material and Debye temperature. For the rest of the interfaces, two equations were used for calculating these

two parameters. They plotted two diagrams of interfacial thermal resistance versus the ratio of Debye temperature and average sound velocity (See Fig. 1.13).

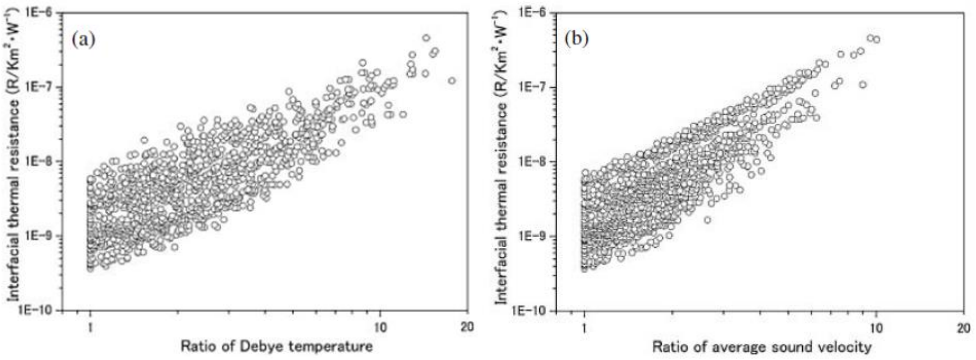

Fig. 1.13 Interficial Thermal Resistance vs Ratio of Debye Temperature and Sound Velocity [41]

The conclusion was that the relation between interfacial thermal resistance and the ratio of average sound velocity is similar to that of the ratio of Debye temperature. For a material system composed of high and low Debye temperature materials, a high interfacial thermal resistance also showed up. Commonly, low interfacial thermal resistances are composed of materials with high and similar Debye temperatures. See Fig. 1.14, blue pixels represent low interfacial thermal resistance which is around 10^{-10} K m^2/W, such as diamond and diamond interfacial thermal resistance. While high thermal resistance happens in dissimilar interfaces and one of the components is of low Debye temperature, such as diamond and Pb interface.

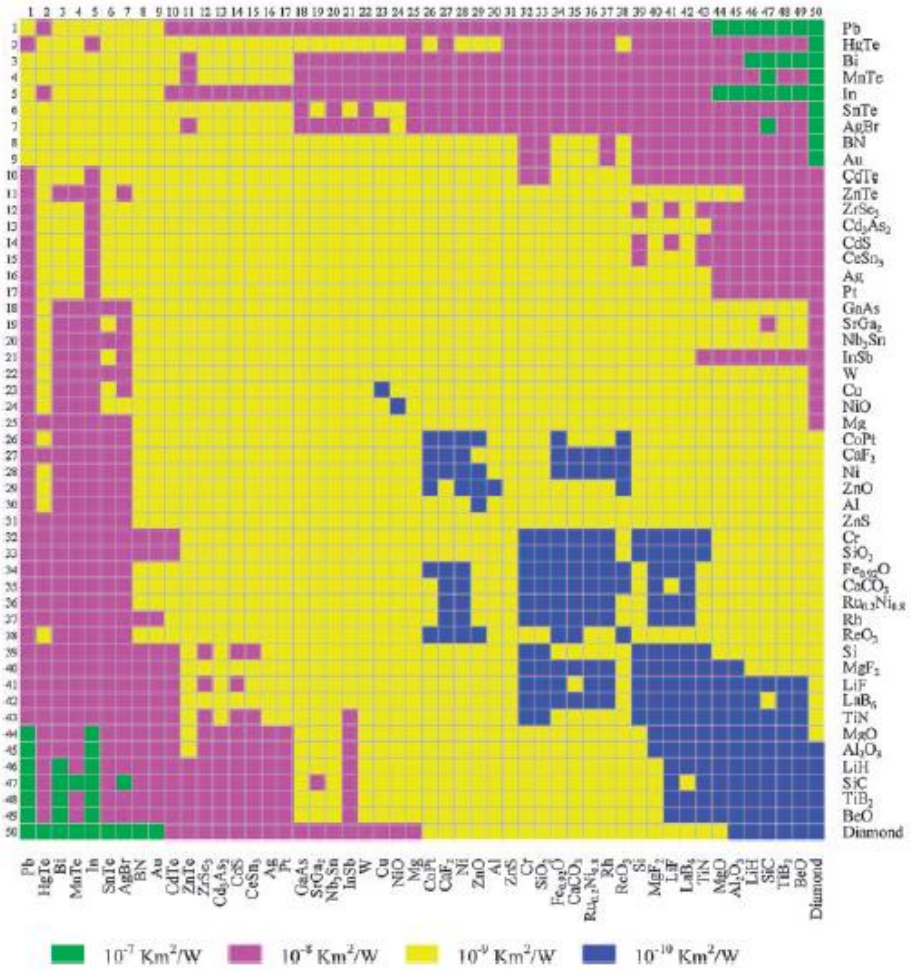

Fig. 1.14 Map of Interfacial Thermal Resistance [41]

This work demonstrated how contact interfaces relate to the thermal property of two adjacent material. So far, interfacial thermal resistance is still restricted to theoretical research, new technique or models should be developed to measure the interfacial thermal resistance values.

CHAPTER 2

2.1 Techniques for Thermal Conductivity Measurements

2.1.1 Scope of Thermal Measurements

Conventional thermal conductivity measurement techniques are dedicated for large scale material measurement, and several methods have been utilized for decades. Some of them are maturely developed, but some newly proposed are still under exploration and development. So far, no single method is appropriate for all kinds of material. Commonly, methods for measuring thermal conductivity are summarized as steady-state method, frequency-domain method and time-domain method. Further, we can separate them into methods for measuring bulk material and thin film material. Thin film measurement can be further divided into in-plane and cross-plane measurement. Sometimes, thin film measurement in cross-plane also available on bulk material due to the penetration depth can sample a deep enough thickness to be characteristic of the bulk material. A summarized table (See Table 2.1) includes methods for measuring thermal conductivity:

Table 2.1 Common Thermal Conductivity Measurements on Bulk Materials and Thin Film [42]

	Bulk material	Thin film
Steady-state	Absolute technique; Comparative technique; Radial heat flow method; Parallel conductance method	Steady-state electrical heating methods
Transient (frequency-domain)	Pulsed power technique	***3ω* method**; Frequency-domain thermoreflectance (FDTR) technique
Transient (time-domain)	Hot-wire method (needle-probe method); **Laser flash method**; Transient plane source (TPS) method	Time-domain thermoreflectance (TDTR) technique

Steady state method is a fundamental method for measuring thermal conductivity, based on the principle that a certain temperature gradient on the material generates a measurable heat flux in the material. This method mainly based on Fourier's law. The related equations are: [42]

$$k = \frac{QL}{A\Delta T} \tag{9}$$

$$Q = p - Q_{loss} \tag{10}$$

Q: The amount of heat flowing through the sample, it is calculated by using the heating power at heat source side p and subtracted by intrinsic heat loss Q_{loss};

L: Distance between temperature sensors;

ΔT: Temperature difference between sensors;

A: Cross-sectional area of the sample.

Drawbacks of steady state method including:

1) Samples are relatively large (at least in centimeter scale)
2) Measuring time is normally longer, sometimes it takes a few hours to reach steady state.

Therefore, this method is not a suitable for measuring ceramic materials but still doable. For low thermal conductivity material, heat reluctantly transfers from one side to another and it takes even longer time.

Specific for ceramic materials, three representative techniques are worthy to be mentioned, Laser Flash Analysis (LFA), Time-domain Thermoreflectance (TDTR) and a

newly developed method Scanning Thermal Microscopy (SThM). The first two methods are time-domain types. A new method not commonly used for ceramics set frequency as independent variable and is called the 3ω method. This is the method we want to expand to measure thermal conductivity of ceramic materials. Each method will be briefly introduced and the 3ω Method will be highlighted.

2.1.2 Laser Flash Analysis (LFA)

Laser flash technique is used for measuring thermal diffusivity instead of thermal conductivity. In addition, to get thermal conductivity information we need to measure the other two parameters, heat capacity and thermal expansion. [24] The relation is shown below:

$$k = \rho\, C_p\, D_{th} \tag{11}$$

k: Thermal conductivity, W/m·K;

ρ: Mass density, kg/m^3;

C_p: Heat capacity, J/kg·K;

D_{th}: Thermal diffusivity, m^2/s,

Geometric measurement plus Archimedes' Method are recommended to get an accurate sense of sample density. Generally, a micrometer is necessary for measuring the dimensions of a sample and calculating geometric density. To exclude the open pores near surface, Archimedes' Method should be performed afterwards. If these two values are close, it means less open pores exist near the sample surface. Most of the time, ceramic materials' density is higher than 95% dense from Archimedes' Method. Although ceramic

material is not sensitive to temperature changes, a slight thermal expansion still intrinsically exists in the material. Thus, the density variation should be considered to get thermal expansion coefficient. Dilatometry is the technique for measuring thermal expansion information with respect to temperature change. [43] For most of the materials, thermal expansion shows a linear relation with temperature. Therefore, a coefficient will be obtained from this technique. Fig. 2.1 is a schematic diagram of Dilatometry measurement system. When temperature heats up on both reference material and sample, expansion quantities are measured by two separate displacement sensors connect to a PC.

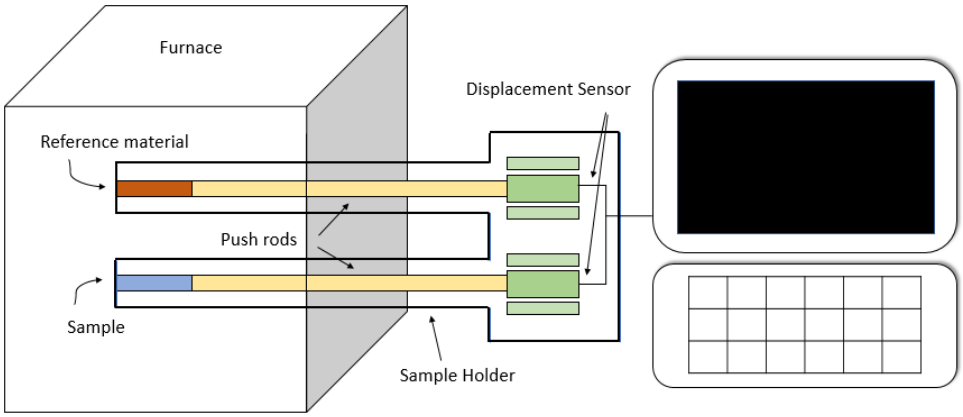

Fig. 2.1 Schematic Diagram of Dilatometry Apparatus

Differential Scanning Calorimeter (DSC) dedicates for material heat capacity measurement. The principle is by measuring the different amount of heat when heat up a sample and reference material as a function of temperature. [44] Maintain the sample and reference material at the same temperature all the time during measurement. Heat capacity of reference material is a known parameter. Linearly increase both reference and target sample holders' temperatures as a function of time, a computer can record the amount of heat that sample needs to keep the temperature consistent with reference sample

temperature. The result from dividing heat supplies by the resulting temperature increases is the heat capacity at certain temperature. Fig. 2.2 shows a computer monitored DSC measurement.

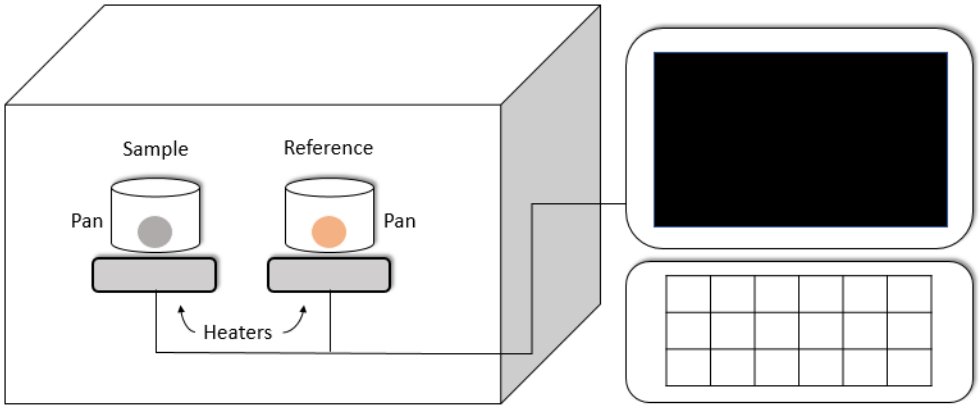

Fig. 2.2 Schematic Diagram of DSC Apparatus

The third instrument involved to get thermal conductivity data is Laser Flash Measurement (LFM), an important apparatus for measuring thermal diffusivity. [45] An energy pulse heat on one side of the parallel-plane material, an infrared detector on the back side monitor the temperature rise as a function of time. If a material has high thermal diffusivity, less time it will need for heat transfer to the other side. Fig. 2.3 shows the LFM apparatus setup. Usually, the samples should not be too thick. To eliminate error and get a relatively reliable data, several samples are required to be measured as comparison.

Before measuring, a thin layer of graphite, usually 5μm, has to be coated on the ceramic sample surface. From polymers to metals to ceramics, materials have huge differences in their physical and chemical properties. Some of polymers or ceramic materials are translucent, therefore, when laser reaches the surface, most of the laser light will penetrate

through the material instead of getting absorbed and heating up the sample. For most metals, laser is likely be reflected. Therefore, a thin layer of graphite can increase emission/absorption property of the material, i.e. increasing the signal-to-noise ratio. While for thin film measurement, a nanometer range of gold layer is applied in order to eliminate light transmission. Before the measurement, a strong light beam tests on the sample and makes sure the sample is totally opaque. The graphite coated sample be dusted (not coated) to make the gold layer is clearly visible. Most ceramic materials are not light translucent unless they are too thin. A graphite layer is essential for ceramic materials to improve laser absorption.

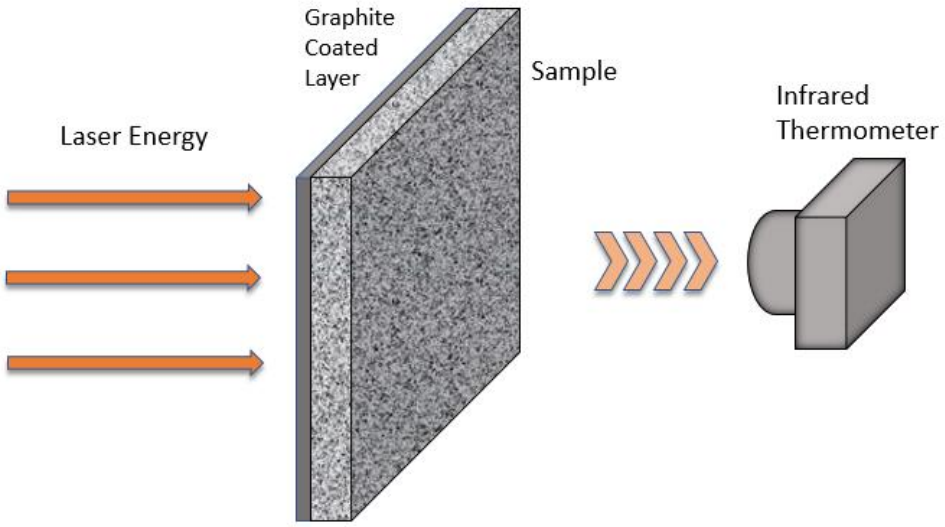

Fig. 2.3 LFM Thermal Diffusivity Measurement

Thermal conductivity calculation by this method may have issues with accuracy, [46] mainly because the result is the product of three uncertain parameters separately measured. Other affected reasons including graphite and substrate contact resistance, contamination and potentially lack of experience in operating. Therefore, extra attention is needed during the measurement.

Another possible reason for differences in thermal measurements is the density deviation. The value usually varies slightly between each sample due to the inconsistent porosity among samples. That is another factor that makes this method inaccurate. To adjust thermal conductivity values of different porosity to a uniform standard, the final thermal conductivity from the calculation should be corrected to the theoretically 100% dense value. *White et al.* [47] proposed an equation to correct the thermal conductivity with some porosity

$$\lambda_{TD} = \frac{\lambda_{exp}}{1-3/2\ (1-p)} \tag{12}$$

λ_{TD} and λ_{exp} are thermal conductivity value for the theoretically dense specimen and experimental value, respectively, and p is average porosity of the samples. However, the definition of p is not correct, since when porosity equals to 0 or a little bit higher than 0, the denominator is a negative value. Therefore, p represents relative density and 1-p should be porosity. Another paper by *Kingery et al*. [48] thermal conductivity was corrected using:

$$\mathrm{k_s} = \frac{k_m}{1-P_v} \tag{13}$$

Where k_s is the solid thermal conductivity, k_m is measured thermal conductivity and P_v is the volume pore fraction. This equation shows that if measured thermal conductivity is a constant, solid thermal conductivity has an inverse relation to the porosity value. Another two equations for correction are *Loeb Equation* [49] and *Maxwell-Eucken Equation*:

$$K_P/K_{100} = 1 - \alpha P \tag{14}$$

$$\mathrm{K}_p/K_{100} = (1-P)/(1+\beta P) \tag{15}$$

Similarly, K_p is the effective conductivity of the porous material, K_{100} is the 100% densified material, P is the pores volume fraction. α and β are two factors mostly relying on the shape and distribution of the pores.

From several proposed equations, we can conclude that K_p / K_{100} ratio has some relation to *(1-P)*. But no single equation applies for all the porous medium, most of the corrected values are approximated when porosity is relatively low.

2.1.3 Time-Domain Thermoreflectance Method (TDTR)

Unlike the Laser Flash Method, which mostly focuses on bulk material, TDTR is more applicable and utilized widely on thin film materials (up to hundreds of nanometers thick). [42] The idea behind this method is that by measuring reflectivity as a function of temperature on the surface, we can get thermal conductivity of the materials.

A sample is heated up by a laser pulse perpendicular to the material surface. Another laser gun is set at some angle relative to the normal vector and use a laser to heat the same spot on the sample surface. Due to the localized heating, the material generates a localized thermal stress, which induces an acoustic strain pulse at the interface. A portion of the pulse penetrates into the material, while the rest reflects with carrying the characteristic information of the interface. [50] Symmetrically set a probe detector with the same angle on the other side to monitor the reflected wave. The reflectivity is measured with respect to time, thus, this method is also one of the time-domain techniques. The data received should be matched with coefficient in the theoretical model, from that we can get thermal property information, most importantly, thermal conductivity. A schematic diagram shows the major components in the TDTR system.

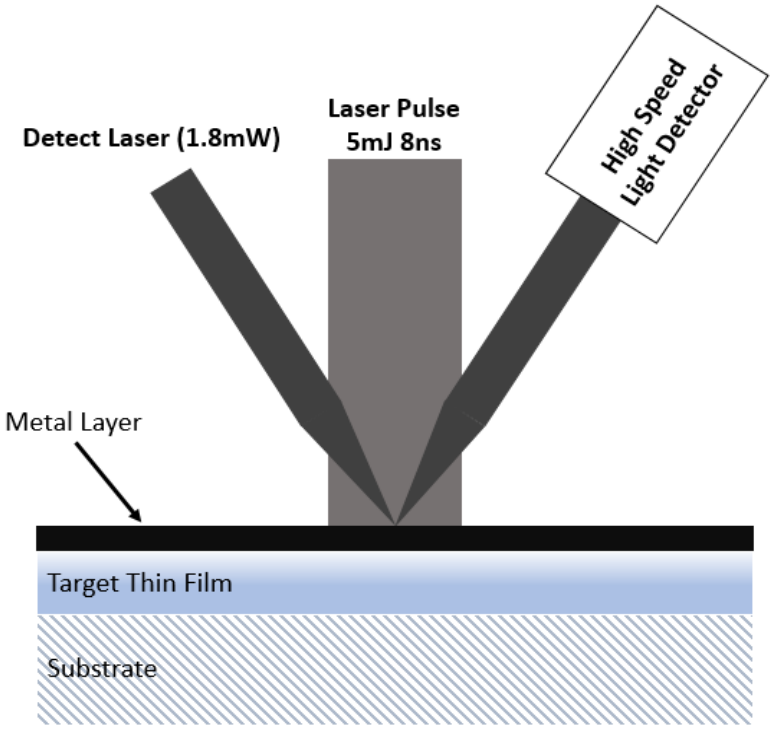

Fig. 2.4 TDTR Schematic Diagram [51]

The metal layer on thin film has the similar function as the graphite layer on the sample surface in Laser Flash Analysis. It's used for increasing sample's emission/absorption property, that is signal-to-noise ratio.

Advantages [42, 50, 51] include 1) No direct contact on the sample surface, 2) Quick heat up, 3) *In-situ* measurement, 4) No ambient temperature requirement.

However, to get appropriate result, 1) A vacuum environment is required so that less heat dissipated by convection. 2) Make samples' feature as similar as possible. Most methods are based on mathematic models, controlling dimensions accuracy and surface roughness is a change for people new to this field. 3) Rigorous measurement condition, a darkroom is preferable. 4) High expense on system building up and maintenance.

2.1.4 Scanning Thermal Microscopy (SThM)

TDTR technically belongs to Far-field Optical Thermometry, which has some intrinsic defects in this type of technique. Low spatial and thermal resolutions, disrupted by ambient air when heating up, need specific operation experience, etc. [52] To increase resolution and accuracy, a novel technology has been developed from Scanning Tunneling Microscopy (STM) and Atomic Force Microscopy (AFM). This technique belongs to the Near-field Microscopy category, which studies the short-range interaction between a fine tip and sample. The interaction can be either static or dynamic depending on the information a microscope subjected to obtain. [53]

Scanning Tunneling Microscopy (STM) and Atomic Force Microscopy (AFM) are two different microscopies for sensing atomic-scale topography. STM depends on the voltage applied on the tip. The mechanism is that when current starts to flow between the gap and move the tip up and down to keep the current constant, the tip's movement can be translated into the surface image. Nevertheless, AFM is based on Van Der Waal's force between the tip and surface atoms. Therefore, AFM can readily image dielectric material while STM cannot.

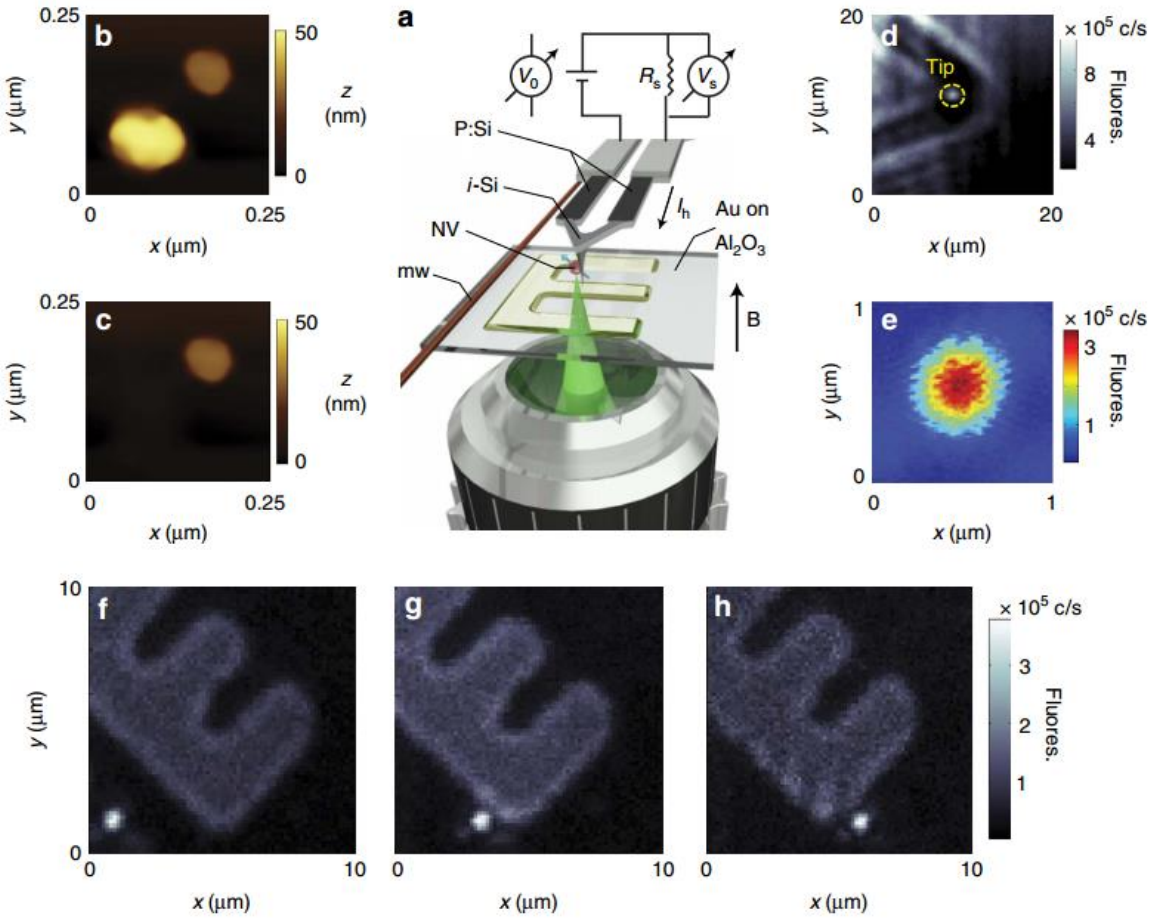

Fig. 2.5 Scanning Thermal Microscopy (a) System setup configuration. (b, c) AFM image. (d) Fluorescence image of the cantilever end and tip. (e) Zoomed confocal image of the NV centre in d. (f-h) Sequential fluorescence images of the nanoparticle [53]

Based on these mechanisms, STM/AFM-based scanning thermal microcopies were created. Basically, the probe mounted on a cantilever heated up with a laser beam leads to a temperature gradient and a heat flux between the gap. Similar to thermocouple mechanism, by keeping another end at reference temperature, one can monitor the heat flux at the tip and transform into the thermal property map on sample surface. A significant benefit from this method is the high spatial resolution, which plays an important role in low dimensional materials. However, a fatal disadvantage is that the fabrication of the tip cost a lot, much more caution is required during designing and operating. [52]

2.2 *3ω* Method

2.2.1 *3ω* Method Introduction

The *3ω* method is the key measurement we want to set up and apply on our ceramic materials due to its succinct development these years. So far, although the *3ω* method has been developed and explored for decades, unlike the other methods, this technique currently has not been commercialized, due to its complexity. Depending on the type of target material, the *3ω* system has to adjust some of the components either in sample preparation or measurement parameter settings.

In the early 20th century, *3ω* original study was primarily focus on the short lifetime of a metal filament, which generally was used in incandescent light bulbs. At the beginning, thermal diffusivity was of interest. With the development of this technique, this method later applied on measuring liquids, dielectric solids, with a thin planar metal filament attached on the surface of interest. [54]

In 1987, *Cahill* [55] first reported using *3ω* method to measure thermal conductivity. With the help of micro fabrication, in the late 20th century, scientists had the ability to make the metal strip even narrower and thinner and bring the experimental setting close to a mathematical model. Fig. 2.6 shows schematic *3ω* electrode measurement.

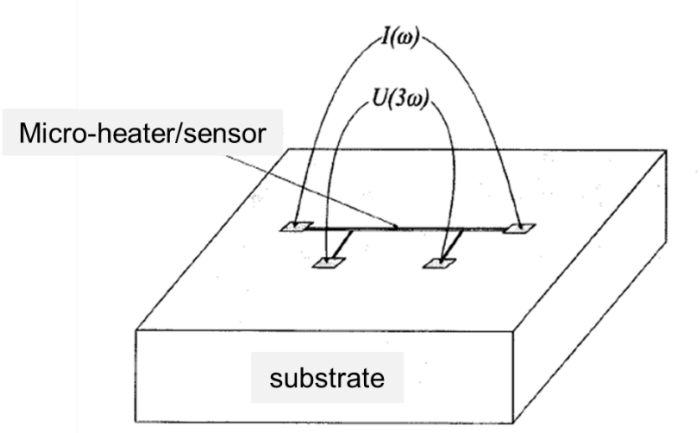

Fig. 2.6 Schematic Arrangement of a *3ω* Experiment

The substrate is the target material for measuring. The reason that this method is called *3ω* is that when providing a signal with a frequency of *1ω*, the resistance of the heater will generate *2ω* oscillating electrical resistance. In turn, a weak third harmonic voltage signal appears on the heater line but buried by other voltage information. The system goal is to 'extract' that *3ω* signal, which amplitude and phase can later be used for calculating thermal conductivity. The primary mathematical derivation is listed below for showing where is the 3rd harmonic voltage from.

An alternative current source provides a driving current *I(t)* on the heater, where I_0 is the amplitude of a sinusoidal current, ω is angular frequency, t is time.

$$I(t) = I_0 sin\omega t \tag{16}$$

Due to the resistance of the heater, Joule heating leads to a *2ω* heating power *P(t)* generates on the heater. R is the heater resistance.

$$P(t) = R \cdot I_0^2 sin^2 \omega t \tag{17}$$

$$= 0.5 I_0^2 R(1 - cos2\omega t)$$

$$= 0.5I_0^2R - 0.5I_0^2Rcos2\omega t$$

Therefore, temperature vibrates at the frequency of 2ω, which leads to the resistance of the heater vibrates correspondingly. dR/dT is temperature coefficient of resistivity. $\Delta T_{2\omega}$ is temperature vibration in 2ω.

$$R = R_0 + \left(\frac{dR}{dT}\right)\Delta T_{2\omega} \tag{18}$$

$$= R_0 + (\frac{dR}{dT})\Delta T cos(2\omega t + \varphi)$$

The present of φ is because of temperature delay when an oscillating power on a resistance. This two oscillating profiles cannot appear synchronously. So far, the driving current oscillates in a frequency of 1ω and resistance changes in 2ω. Using the product and sum formulas we can calculate the voltage on the heating wire, in other words, the 3rd harmonic signal.

$$V = IR = I_0\, sin(\omega t) \cdot \left[R_0 + \left(\frac{dR}{dT}\right)\Delta T cos(2\omega t + \varphi)\right] \tag{19}$$

$$= I_0\, R_0 sin(\omega t) + I_0 \left(\frac{dR}{dT}\right)\Delta T cos(2\omega t + \varphi)\, sin(\omega t)$$

$$= V_0\, sin(\omega t) + \frac{V_0}{R_o}\left(\frac{dR}{dT}\right)\frac{\Delta T}{2}[sin(3\omega t + \varphi) - sin(\omega t + \varphi)]$$

$$= \left[V_0\, sin(\omega t) - \frac{V_0}{R_0}\left(\frac{dR}{dT}\right)\frac{\Delta T}{2} sin(\omega t + \varphi)\right] + \frac{V_0}{R_0}\left(\frac{dR}{dT}\right)\frac{\Delta T}{2} sin(3\omega t + \varphi)$$

$$= V_{1\omega}\, sin(\omega t + \theta) + V_{3\omega} sin(3\omega t + \varphi)$$

Fig. 2.7 visualizes the relationship between current and voltages. A thermal transfer function Z is introduced for relating the average temperature rise of a heater θ_{avg} to the

heat input Q. $\otimes$ denotes convolution and Z_t is the inverse Fourier transform of Z. R_{e0} is the electrical resistance at zero current and α has the similar function as dR/dT which denotes temperature coefficient of resistance.

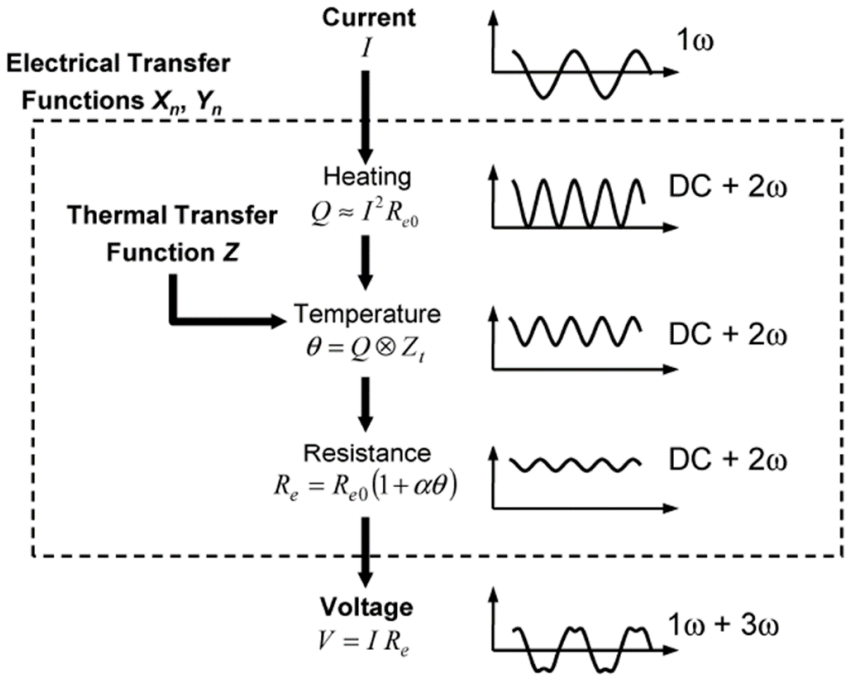

Fig. 2.7 Schematic Relationship between sinusoidal Current and Voltages and Thermal Transfer Function [58]

To get thermal information from 3rd harmonic voltage, *Dames et al.* [59] derived the analogous results for the more general case of a sinusoidal current with a *dc* offset. See Eqn. 20 [59] for the expression of rms voltages $V_{n\omega,rms}$ at the various harmonics $n\omega$.

$$\frac{V_{n\omega,rms}}{2\alpha R_{e0}^2 I_{1\omega,rms}^3} = X_n(\omega_1,\eta) + jY_n(\omega_1,\eta) \tag{20}$$

α is temperature coefficient of resistance, $\alpha(T)= (1/R_{e0})/(dR_{e0}/dT)$. R_{e0} as mentioned previously is the electrical resistance at zero current at temperature being measured, $R_{e0}(T)$ =lim $[V_{1\omega}/I_{1\omega}]_{I\to 0}$. $I_{1\omega,rms}$ is the root mean square of fundamental electrical current, $I_{1\omega,rms}= I_{1\omega} / \sqrt{2}$. $j =\sqrt{-1}$, $\eta = I_{dc}/ I_{1\omega}$ and $X_{n\omega}$ and $Y_{n\omega}$ are the in-phase and out-of-phase

electrical transfer functions, respectively. See Table 2.2 for eight transfer functions at different harmonics.

Table 2.2 0ω, 1ω, 2ω and *3ω* electrical transfer functions [59]

Harmonic n	In-phase electrical transfer function $[X_n(\omega_1, \eta)]$	Out-of-phase electrical transfer function $[Y_n(\omega_1, \eta)]$
0	0	$\eta\sqrt{2}\{\frac{1}{2\alpha R_{e0} I_{1,\mathrm{rms}}^2}+[\eta^2+(1/2)]Z(0)+\mathrm{Re}[Z(\omega_1)]\}$
1	$\frac{1}{2\alpha R_{e0} I_{1,\mathrm{rms}}^2}+[\eta^2+(1/2)]Z(0)+2\eta^2\,\mathrm{Re}[Z(\omega_1)]+(1/4)\mathrm{Re}[Z(2\omega_1)]$	$(1/4)\mathrm{Im}[Z(2\omega_1)]+2\eta^2\,\mathrm{Im}[Z(\omega_1)]$
2	$\eta(1/2)\{\mathrm{Im}[Z(2\omega_1)]+2\mathrm{Im}\,[Z(\omega_1)]\}$	$-\eta(1/2)\{\mathrm{Re}[Z(2\omega_1)]+2\mathrm{Re}[Z(\omega_1)]\}$
3	$-(1/4)\mathrm{Re}[Z(2\omega_1)]$	$-(1/4)\mathrm{Im}[Z(2\omega_1)]$

These transfer functions generally apply to any system with a line heater for measuring temperature. *Re* means the in-phase or 'real' component and *Im* is out-of-phase or 'imaginary' component. Thermal property information is contained in both *X* and *Y* signals of the 3rd harmonic and also they are directly proportional to the real and imaginary components of the thermal transfer function. From Table 2.2 we have:

$$X_3 = -\frac{1}{4} Re\{Z(2\omega)\} \tag{21}$$

Where Z (2ω) is the thermal transfer function at frequency 2ω. The mathematical model was derived by *Carslaw* [56] in *Conduction of Heat in Solids,* in which he described a theoretical thermal profile in the scenario. Two assumptions as the preconditions: 1) Substrate is a semi-infinite solid relative to the heater; 2) Heater is an ideal heating source.

$$\Delta T(r) = \frac{P}{l\pi k} \cdot H_0(qr) \tag{22}$$

$$r = \sqrt{x^2 + y^2} \tag{23}$$

ΔT(r): Temperature oscillation with respect to heat diffusing distance.

P: Heating power

r: Temperature Oscillating distance

l: Length of the heater

k: Thermal conductivity

H_0: Zeroth order Bessel function.

$1/q=(D/i2\omega)^{1/2}$: Thermal penetration depth.

D: Thermal diffusivity

However, an infinitely narrow line cannot be achieved in reality. Therefore, *Cahill* [55] came up with a finite width heating line on a semi-infinite solid substrate. The approximately expression of temperature oscillation ΔT with respect to frequency ω is shown in Eqn. 24 [55].

$$\Delta T = \frac{P}{l\pi k} \cdot [\frac{1}{2} ln \frac{D}{r^2} - \frac{1}{2} ln(2\omega) + ln2 - 0.5772 - \frac{j\pi}{4}] \quad (24)$$

Similarly, *P* is the heating power, *l* is the length of the heater, *k* is the thermal conductivity of interest, *D* is thermal diffusivity and *r* is the temperature oscillating distance. Since thermal transfer function relates temperature rise to heat input, we can obtain an expression for thermal transfer function after unifying those scattered constants into one value. See Eqn. 25.

$$\mathrm{Z} = -\frac{1}{2\pi kL} [ln(2\omega) + \frac{j\pi}{2} + const.] \quad (25)$$

Constant is an unknown real constant, by plugging in to the Eqn. 21: [59]

$$X_3 = \frac{1}{8\pi kL} [\ln(2\omega) + const.] \quad (26)$$

From Eqn. 20 we have the in-phase voltage equation for 3rd harmonic:

$$X_3 = \frac{V_{3\omega,ip}}{2\alpha R_{e0}^2 I^3} \tag{27}$$

Relate Eqn. 26 to Eqn. 27 then we have:

$$\frac{V_{3\omega,ip}}{2\alpha R_{e0}^2 I^3} = \frac{1}{8\pi kL}[\ln(2\omega) + const.] \tag{28}$$

Rearrange:

$$V_{3\omega,ip} = \frac{\alpha R_{e0}^2 I^3}{4\pi kL}[\ln(\omega) + \ln(2) + const.] \tag{29}$$

Take differential of $V_{3\omega,ip}$ with respect to $\ln(\omega)$:

$$\frac{\partial V_{3\omega,ip}}{\partial \ln(\omega)} = \frac{\alpha R_{e0}^2 I^3}{4\pi kL} \tag{30}$$

Therefore, thermal conductivity of in-phase component expression is:

$$k = \frac{\alpha R_{e0}^2 I^3}{4\pi L}\left(\frac{\partial V_{3\omega,ip}}{\partial \ln(\omega)}\right)^{-1} \tag{31}$$

Similarly, thermal conductivity of out-of-phase component expression is:

$$k = \frac{\alpha R_{e0}^2 I^3}{8L V_{3\omega,op}} \tag{32}$$

Thus, either we need to measure the 3rd harmonic voltage with respect to frequency or measure the accurate 3rd harmonic voltage, we can get thermal conductivity information from this technique. From previous experience by *Cahill* [55], calculation from in-phase component is more accurate and stable than out-of-phase component.

Ever since the *3ω* method was reported, this technique was developed and applied widely on different types of material. From bulk materials measurement to thick films then to thin film, later to liquid, carbon fiber and nanomaterials, *3ω* method played important role in measuring thermal conductivity, especially in 'tiny scale' material, such as microelectronic material, biomedical materials, etc.

Several essential equipment need to be used in *3ω* measurement system. A schematic diagram of conventional *3ω* system is shown in Fig. 2.8. It has some difference compare to the system we are using, since some components are replaced by integrated components on circuit board.

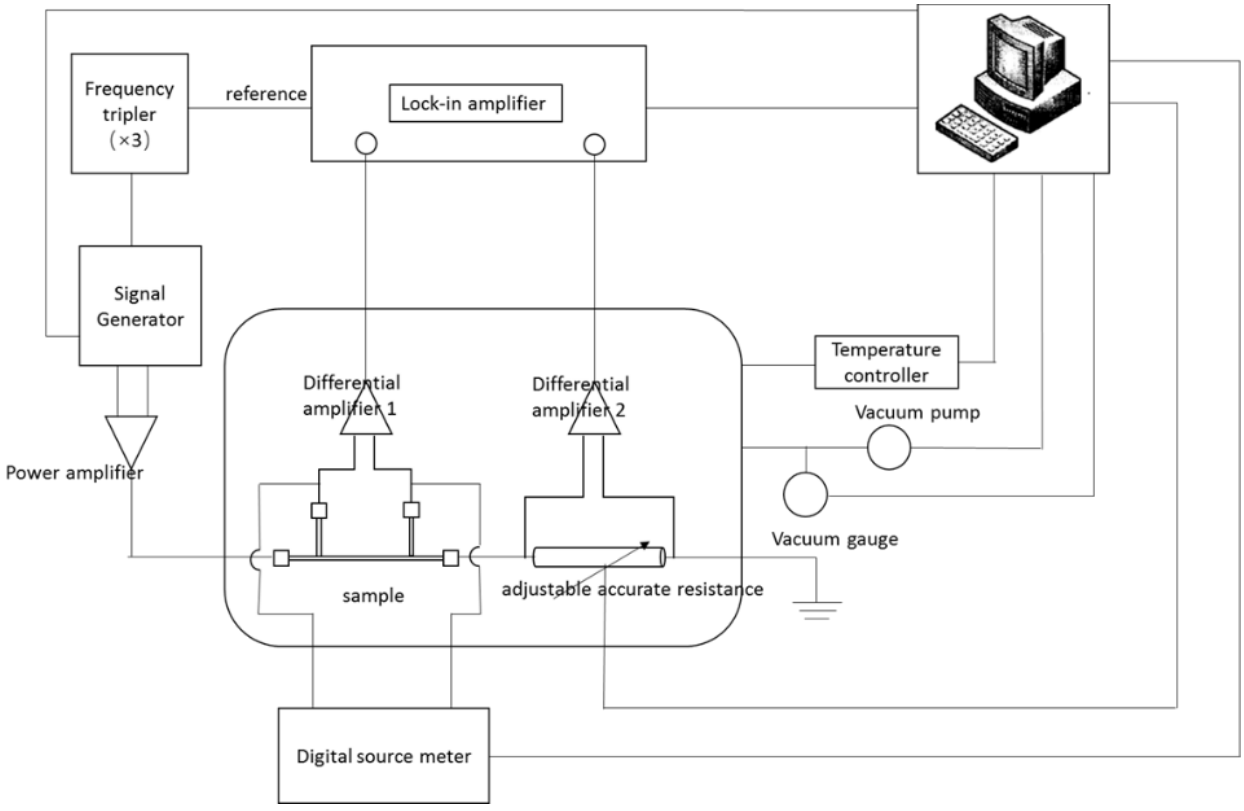

Fig. 2.8 Schematic Diagram of Conventional *3ω* System

A lock-in amplifier is an essential part of the system. Generally, a lock-in amplifier is used for measuring weak *3ω* signal and it also can be used as a signal generator. For some of the research groups, they prefer to use an external signal generator as a signal source, together with a frequency tripler, the frequency of the fundamental signal is tripled and input into lock-in amplifier as a reference. Sample and an adjustable accurate resistance are connected in series and differentially input the voltage information into lock-in amplifier, this part is simplified with a dummy resistor printed on an integrated circuit board in our system. But conventional system is easier to understand how *3ω* system works. A furnace or hot plate is required for maintaining the sample at a different temperature. All these instruments are monitored by a PC. Generally, as long as we get a frequency reading from lock-in amplifier and detect the 3rd harmonic signal, we can plug the data into the equations and get thermal information.

2.2.2 Purpose for Using *3ω* Method

Particularly for ceramic materials, several advantages become the reasons that we are attracted by the *3ω* method.

First, from the material point of view, ceramic materials are easy to get a really smooth surface after some polishing, and have barely any dimensional changes during temperature changes (up to 750K). Another thing is that different preparation techniques during ceramic preparation may lead to some characteristic variation within just one sample. The good thing for the *3ω* method is that it can represent local information under the wire, with the pushing limit to 50nm. [58] Therefore, multiple points measurement more reliably shows different in the properties in different of the sample.

Secondly, compared to other methods, it does not require an accurate sample size preparation, if we have a pattern mask, we can either use photolithography or evaporation to get a metal wire on the surface. For our wire currently, it's 1mm long, 50μm wide and 100nm thick. The substrate cannot be too thin, but as long as it much larger than mean free path (phonon: 100nm) of the material, the result will be reliable. Therefore, the *3ω* method can still measure a wide thickness range (from 50nm to a few millimeters) of materials.

Third, unlike laser flash method, it only needs to use one face of the sample to measure the thermal property and this makes the setup work easier. Compared to Time-domain Thermoreflectance method, the direct contact measurement eliminates the errors due to air and surface uncertainty.

Fourth, the *3ω* method system is easy to set up. The cost for all the instruments is not so high compared to other thermal property measurement techniques and maintenance expense is also lower than other systems. Less space is required for *3ω* for a system setup in the lab than other techniques.

Briefly summarize the advantages of the *3ω* method, including:

1) Wide application. This method is used from solid to liquid, from thick material to thin material.

2) Accurate. Using a metal strip directly stick on the sample surface can eliminate the uncertainty of remote measurement, for example, laser flash. With few of parameters, we can get thermal conductivity information, avoiding too many factors influencing the results. Since this method is only measuring a small spot on the sample surface, the result can accurately represent characteristics around that spot.

3) Economical. Usually, several electrodes are put on the surface of a sample, therefore, a small volume of sample is sufficient for measuring, not only saves the expense on material but also on the time during sample preparation. And the whole system does not take a lot of space to set up.

4) Flexible. A vacuum environment is not necessary for measuring. Due to the heat generated by driving current is so small, air convection is negligible if operated in a box and it will not influence signal quality too much.

2.2.3 A Brief Review of *3ω* Method

Since the *3ω* method had been first reported by *Cahill* [55], it has been developing for 30 years. Because of the merits of this method, it has been tried on a large amount of materials, especially materials commonly be used in daily life. For ceramic material, specific for nuclear industry ceramic materials, due to its high operating temperature, ceramic materials usually use laser flash method for thermal conductivity measurement. Some related work was done by *Angel et al.* [25] on two-phase ceramic material, to study the influence on the thermal and mechanical property of the second phase. He used a 10nm layer of chromium as an adhesion layer and used photolithography to deposit a gold heater line on top of the chromium layer. The heater was 10μm wide, 250nm thick and 0.5mm long which is the distance in between the inner voltage pads. The oscillating temperature field over a certain length scale known as 'thermal penetration depth', from his work it was estimated from 8.7μm to 47μm with the equation:

$$\lambda = \sqrt{\frac{D}{2\omega}} \tag{33}$$

λ is thermal penetration depth, D is thermal diffusivity and ω is the angular frequency, which he used from 30*Hz* to 890*Hz* in the experiment. 8YSZ with different volumetric percentage of Al_2O_3 and Mullite to form multiphase ceramic materials and measured with *3ω* method. The data was plotted out in Fig. 2.9. Different colors represent corresponding composite.

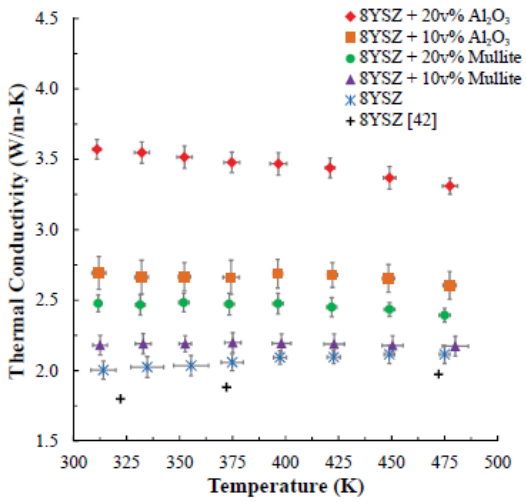

Fig. 2.9 Thermal Conductivity of Different Volume Percent Multiphase Ceramic Materials [25]

Then the paper used OOF2 simulation, Maxwell Garnett model, Bruggeman model and linear Rule of Mixtures as theoretical models to compare with experimental data. For example, 8YSZ with 10vol% and 20vol% Al_2O_3 compare with their modeling values. See Fig. 2.10 for the comparison between these methods.

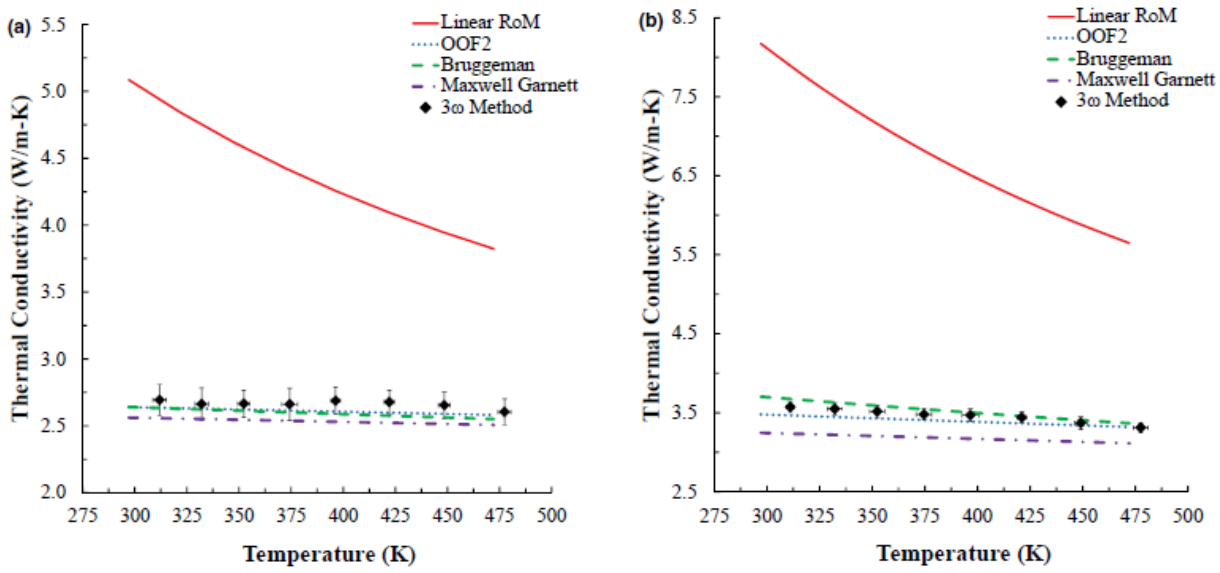

Fig. 2.10 (a)10vol% Al2O3 (b)20vol% Al2O3 Forming Multiphase Ceramic with 8YSZ [25]

The *3ω* method is closed to some of the theoretical values, especially for OOF2. However Linear RoM far deviates from common values, it has the worst agreement with the experimental values. The *3ω* method showed great accuracy in measuring thermal conductivity compare to some theoretical model.

Zhao et al. [42] did research on thermal and electrical characterization on ultra-thin flexible 3YSZ ceramic for electronic packaging technique. The substrate 3YSZ ceramics are 20μm and 40μm. This flexible material can potentially provide higher robustness in manufacturing but also low thermal resistance for power module to avoid heat accumulation in electronic packaging. For thermal conductivity measurement on this material, they also used *3ω* method but with a different design for the electrode (See Fig. 2.11). The width of the heater is 100μm and effective length is 8mm.

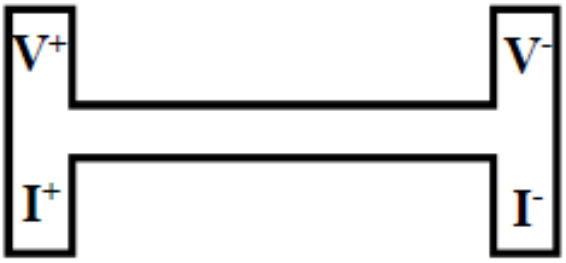

Fig. 2.11 *3ω* Pattern Heater Line [42]

As a comparison, they used Transient Thermo-reflectance (TTR) method (See Fig. 2.12) for measuring thermal conductivity as well. Similar to the TDTR we introduced previously, they used a Si photodiode to collect the reflected laser beam. An oscilloscope was used for recording after amplification.

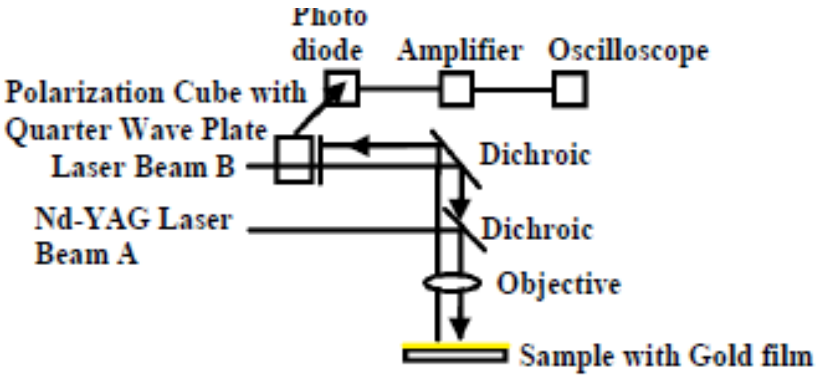

Fig. 2.12 TTR Thermal Conductivity Measurement [42]

The result from *3ω* method showed that flexible 3YSZ thermal conductivity decrease from 3.3 W/m·K to 2.2 W/m·K when the temperature rises from 235K to 600K. The thermal conductivity by the *3ω* method versus temperature is shown in Fig. 2.13.

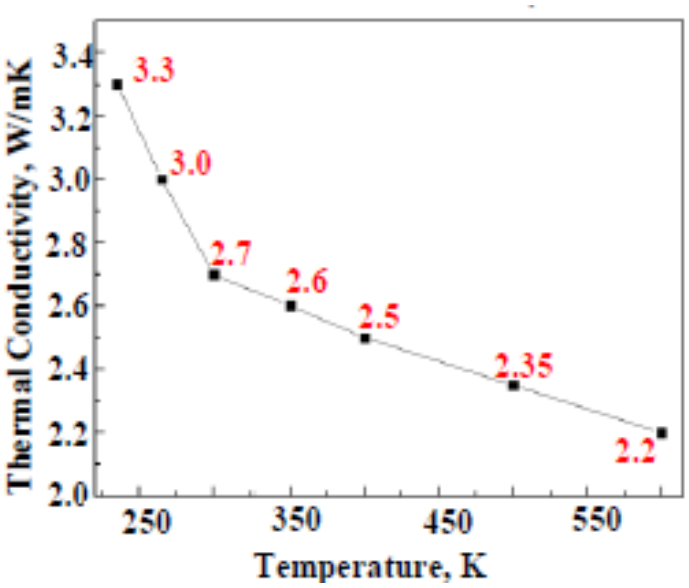

Fig. 2.13 The Thermal Conductivity of 3YSZ by *3ω* Method [42]

For the corroboration technique, the normalized variation along with curve fitted results from the simulation is shown in Fig. 2.14. Both the simulation parameters and curve fitting process determined 3YSZ thermal conductivity was 2.85 W/m· K. The value agreed with *3ω* method well.

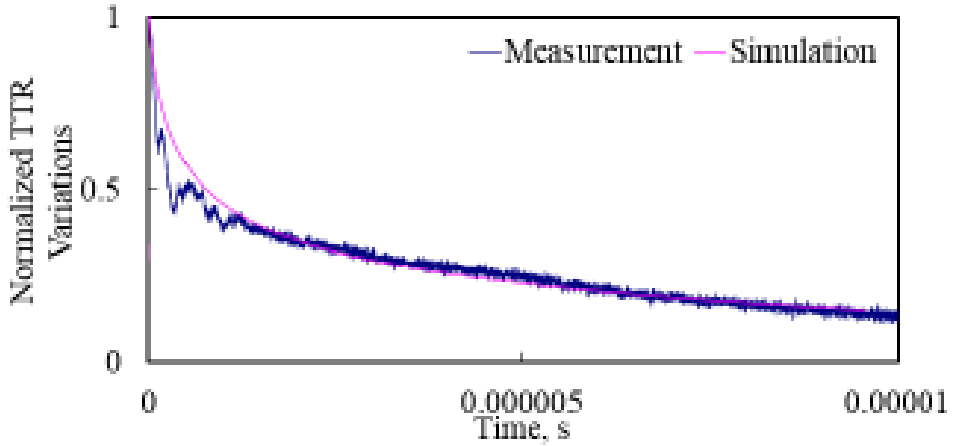

Fig. 2.14 Curve Fitting of TTR Variation with Time of Experimental and Simulation Results [42]

Another research related to *3ω* method was done by *Qiu et al.* [57] on Macroporous polymer-derived SiOC ceramics, a promising, high-temperature insulation material. The thermal conductivity calculates by theoretical formula agree well with the experimental results over a density range from 0.254g·cm^{-3} to 0.533g·cm^{-3}, showed *3ω* method is an accurate method for measuring thermal conductivity. The comparison of theoretical and experimental data was plotted out and shown in Fig. 2.15.

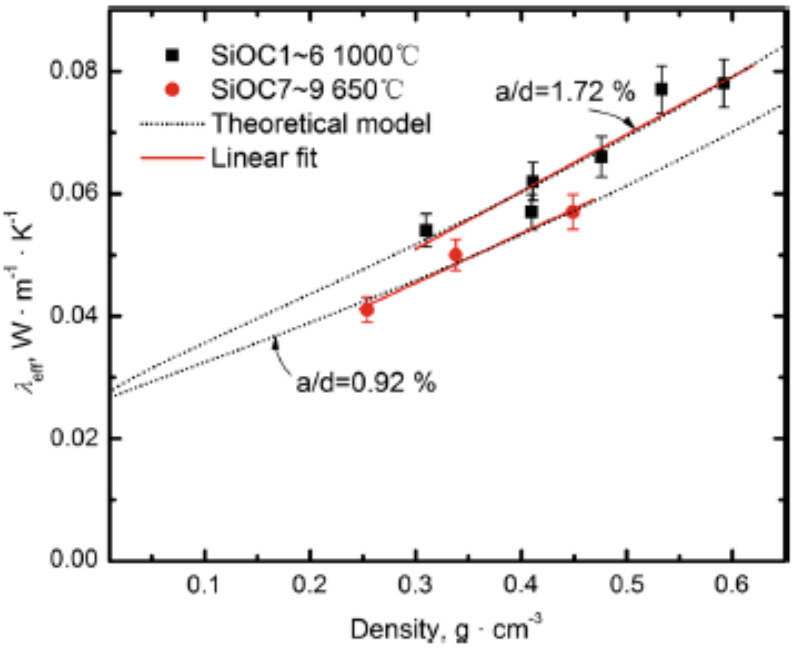

Fig. 2.15 Thermal Conductivity of Theoretical and Experimental Data [57]

For our comparison experiments, laser flash method is suitable for ceramic material and can measure thermal conductivity under high temperature, the sample materials do not have to be polished so well and no contact when measuring, which are great advantages for this method. But there is still some drawbacks such as inaccurate and plenty samples requirement. But we want to compare *3ω* method with laser flash method, in addition, we want to compare these two methods with theoretical values.

2.3 Oriented-Object Finite Element Analysis Version 2 (OOF2)

OOF2 is a free simulation software dedicates for modeling thermal gradient in a composite material released by U.S. Department of Commerce. Most suitable systems for running are Linux and Macintosh OSX, or one can try to use visual machine on Windows operation system.

For 3-phase composite analysis, the SEM images are colorized with 3 different colors representing the three phases and finite meshes adapted to the microstructure of the material. Each phase with a corresponding color are assigned a thermal conductivity value at a certain temperature from literature. For convenience, the top temperature is set 10K higher than the bottom side and the side walls adiabatic. Heat flux in x and y direction is assigned to each node by conjugate gradient method. The result of effective thermal conductivity can be calculated from:

$$k_{eff} = \frac{L_y \cdot Q}{L_x \cdot \Delta T} \tag{34}$$

k_{eff}: Effective thermal conductivity in a composite;

L_y & L_x: Pixels on y direction and x direction;

Q: Heat flux integrated across the bottom boundary;

ΔT: Temperature difference assigned to the top and bottom boundaries.

By assigning different values on those phases at some certain temperature, and setting the boundary temperature to the value of interest, we can obtain thermal conductivity for that composite microstructure. Several representative images from SEM (See Results and

discussion 5) are selected for analyzing to get an average value of effective thermal conductivity.

2.4 Importance of This Work

This work essentially uses advanced technologies to measure thermal conductivity of ceramic materials and from that get a deeper understanding on heat transfer mechanism in ceramics. And together with microscopic characterization, mechanical strength test and irradiation test, we can use the information on how to develop materials with higher durability and tolerance. With the 3ω set-up, we can expand to more materials and hopefully in the future help develop better composite materials with high efficiency and enhanced performance.

CHAPTER 3

3.1 Sample Preparation

A detail ceramic sample preparation procedure can be found in Appendix A. *3ω* method sample preparation including evaporation and thermal conductivity system setup can be found in Appendix B and Appendix C. This section will go through every step in ceramic sample preparation, due to the demand difference, this section only uses *3ω* sample as an example.

Three types of the sample had been prepared. Single phase 8YSZ, large grain 3-phase ceramic and fine grain 3-phase ceramic. 8 mol% YSZ ceramic powder (TOSOH Co. Ltd., Japan). High-purity α-Alumina powder (Taimei Chemicals Co. Ltd., Japan), $MgAl_2O_4$ powder (Baikowski Inter. Corp., NC) were used for preparing single phase and 3-phase ceramics. Szegvari Attritor System (Union Process Inc. Ohio) was used to wet mill powders in Isopropanol for 12hrs each batch. Drying the suspension using a hot plate (Fisher Scientific, New Hampshire) at 65℃ for 12hrs converted the slurry to a solid chunk and use of a pestle to ground the chunk into fine powders. After sieving the ground powders with a sieving machine (Fritsch Co.), the finest powders were collected in glass sample bottles. Silicone Compound (Momentive Performance Materials, NY) and Curing Agent (Momentive Performance Materials, NY) plus Silicone Lubricant (LPS Labs, GA) made cylinder molds. Tamping the mold after filling with enough powders and compressing by Cold Isostatic Pressing (Autoclave Engineers, PA) at 55kpsi for 5mins made small pellets. Sintering was conducted in air under 1550℃ 12hrs for large grain sample and 1325℃ 5hrs for fine grain (Find detail sintering profile in Appendix A) with Rapid Temp Furnace (CM Inc. NJ). Each

sample was weighted with precision mass balance (OHAUS, NJ) and their geometries measured with screw micrometer (Mitutoyo Co. Japan) usually diameter is around 9mm and length is around 10mm. Cut samples with specific geometries (Length of side: 8mm, thickness: 1mm) with a low speed saw (BUEHLER, IL). To create a smooth surface, samples were ground and polished to different finishes from 120 grit abrasive papers to 800 grit abrasive paper (BUEHLER, IL) and variable speed grinder-polisher (BUEHLER, IL). To get a fine finish, monocrystalline diamond suspension (BUEHLER, IL) together with a polishing board (from 6μm to 0.06μm) was utilized. For an extremely fine finish, diamond lapping film (South Bay Technology Inc., CA) can be used as well. It was important to observe the roughness and any residual scratches between each polish step by using an optical microscope function in a hardness tester (Zwick Roell 3212, GA). For SEM, the tube furnace (Thermo Fisher Scientific, MA) was used for thermal etching at 1200℃ for 30mins and sample were cleaned with a sonicator (NEY ULTRAsonik, NY). More details in ceramic sample preparation can be found in Appendix A.

3.2 Characterization

X-ray diffraction (XRD; Rigaku SamrtLab X-ray Diffractometer, Tokyo, Japan) used Cu-k_β radiation as source and scanned from 20° to 100° in 0.02° steps, 1°/min. The microscopic images were performed using FEI Magellan 400 XHR SEM (FEI, Hillsboro, OR). Before running SEM, a thin layer of iridium metal was be deposited on the sample surface (South Bay Technology IBS/e Ion Beam Sputter Deposition System, San Clemente, CA) to prevent electrical charging. The grain size in two dimensions distribution was measured by ImageJ (National Institute of Health). To convert the two-dimensional grain size to the three-

dimensional grain size, a factor of 1.74 should be multiplied. The factor is derived using the mathematical relationship between equiaxed and polyhedron calculation.

CHAPTER 4

Results and Discussion

1. Microstructure and phase characterization

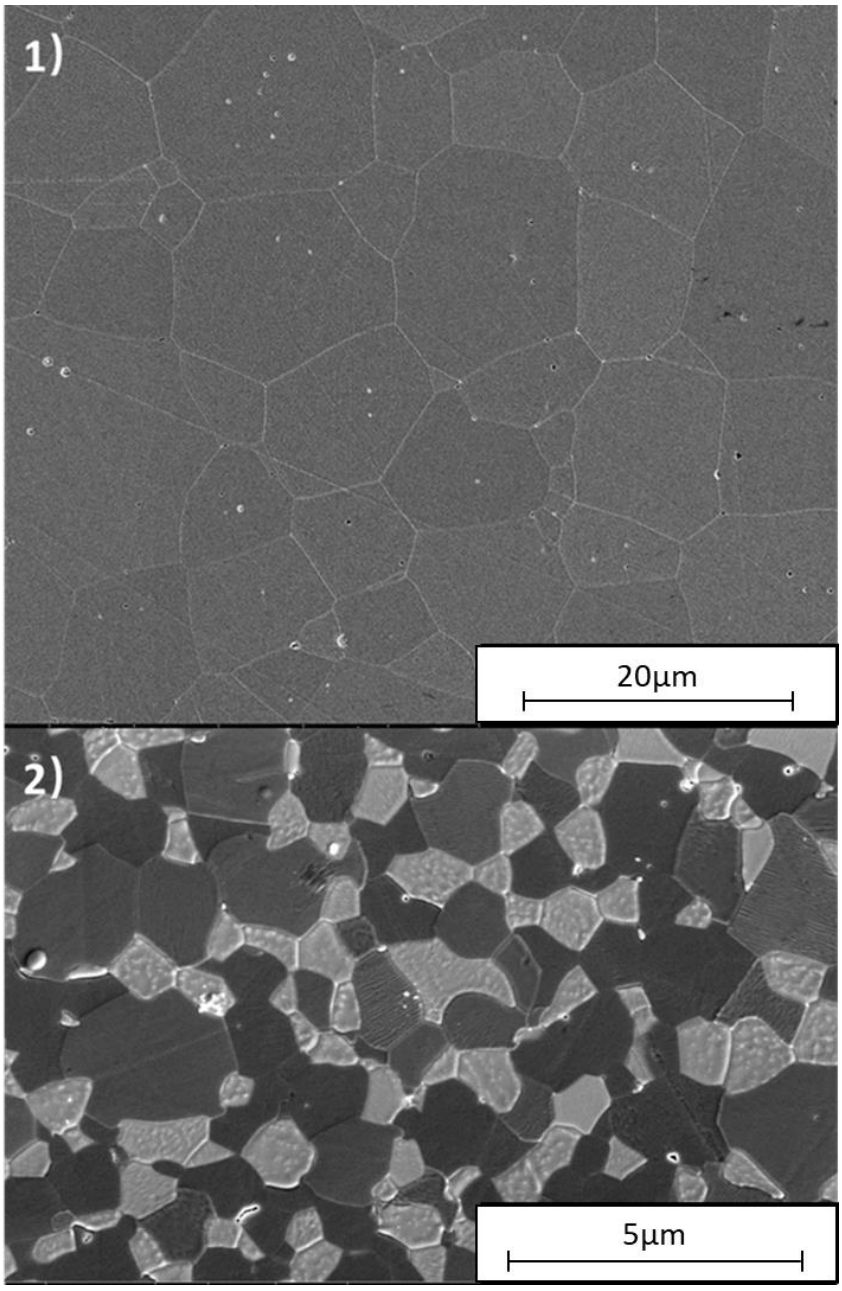

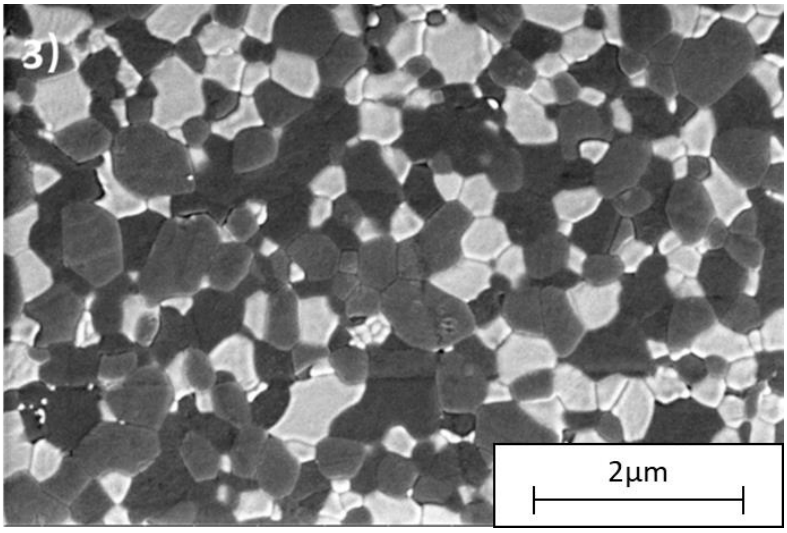

Fig. 4.1 SEM Images 1) 8YSZ; 2) 3-phase Large Grain; 3) 3-phase Fine Grain

The additional phases are significantly effective in reducing the grain size of the material. Based on the Z-contrast in SEM, the heaviest atom phase among the three phases is 8YSZ, therefore the white phase is 8YSZ (See Fig. 4.1). Similarly, the grey phase is Al_2O_3 and dark phase is Spinel. Samples are all above 96% dense (See Table 4.2), the lowest is the 3-phase fine grain sample due to the low temperature and short time in sintering. In 3-phase ceramic material, three different phases are roughly homogeneously distributed in the material, one with larger grain could be the energy threshold for powder agglomeration or mass diffusion is less than the others.

2. Grain Size Distribution

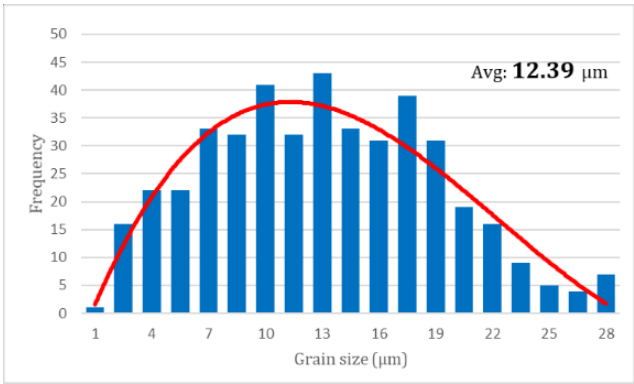

Fig. 4.2 8YSZ Grain Size Distribution

Grain distribution in each phase of 3-phase ceramic material is collected from 10 images and summarized in Table 4.1.

Table 4.1 3-phase Large Grain and Fine Grain Distribution Comparison

	3-Phase Large Grain	3-Phase Fine Grain
8YSZ	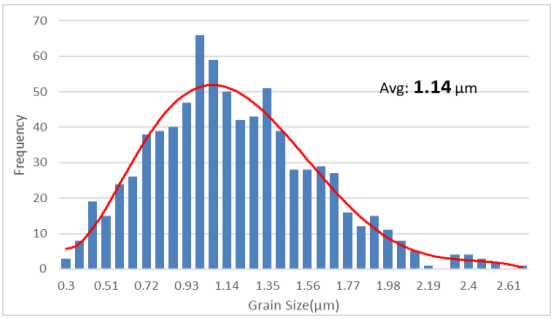	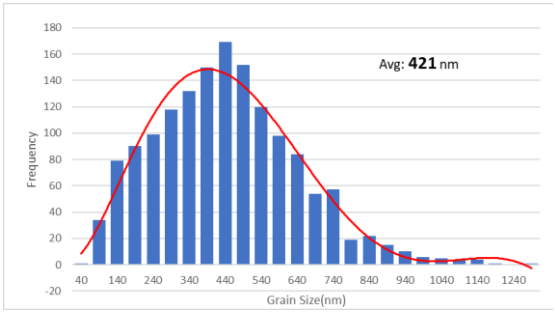
Al_2O_3	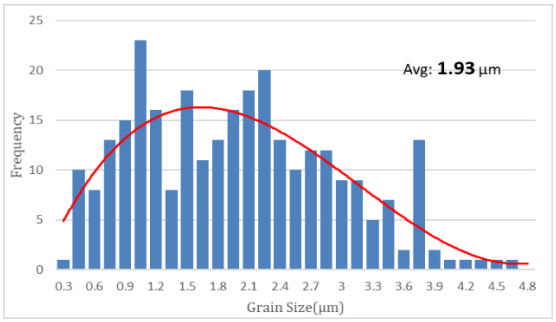	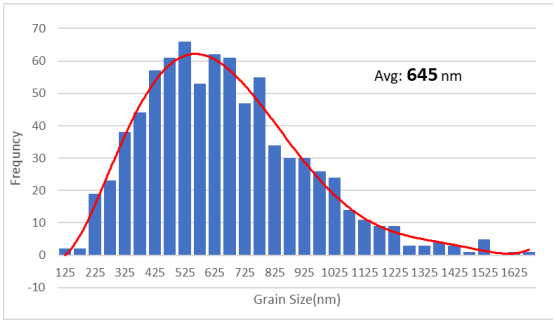
Spinel	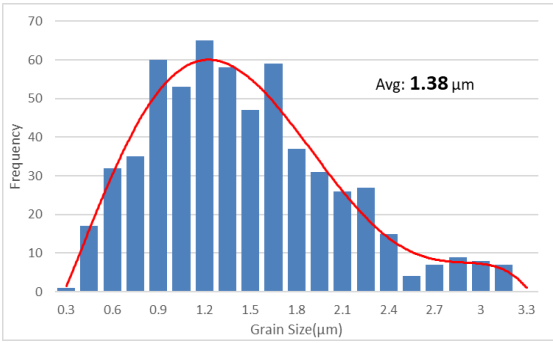	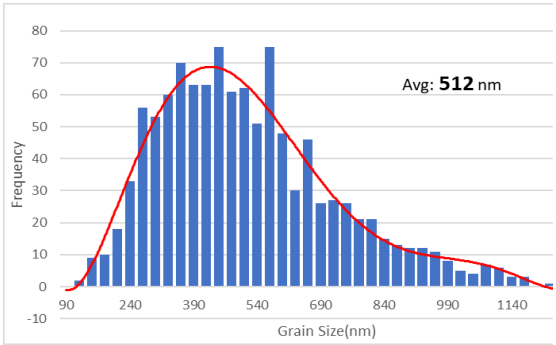
Comp-arison	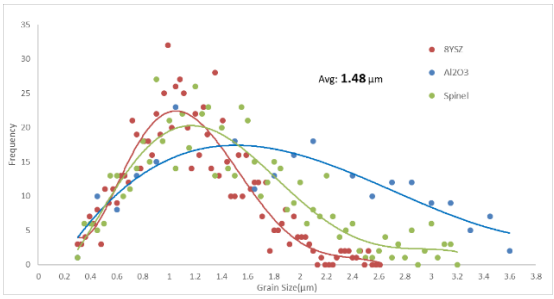	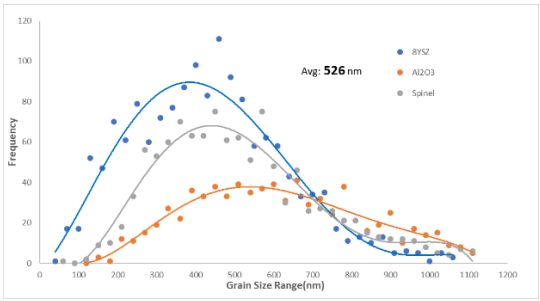

Table 4.2 Theoretical Density, Relative Density and Average Grain Size in 3 Samples

	Theoretical Density (g/cm³)	Relative Density (%)	8YSZ Grain Size (μm)	Al2O3 Grain Size (μm)	Spinel Grain Size (μm)
8YSZ	6.00	98	12.39	-	-
3-phase large grain	4.51	98	1.14	1.93	1.38
3-phase fine grain	4.51	96	0.42	0.65	0.52

3. X-ray diffraction diagram phase check

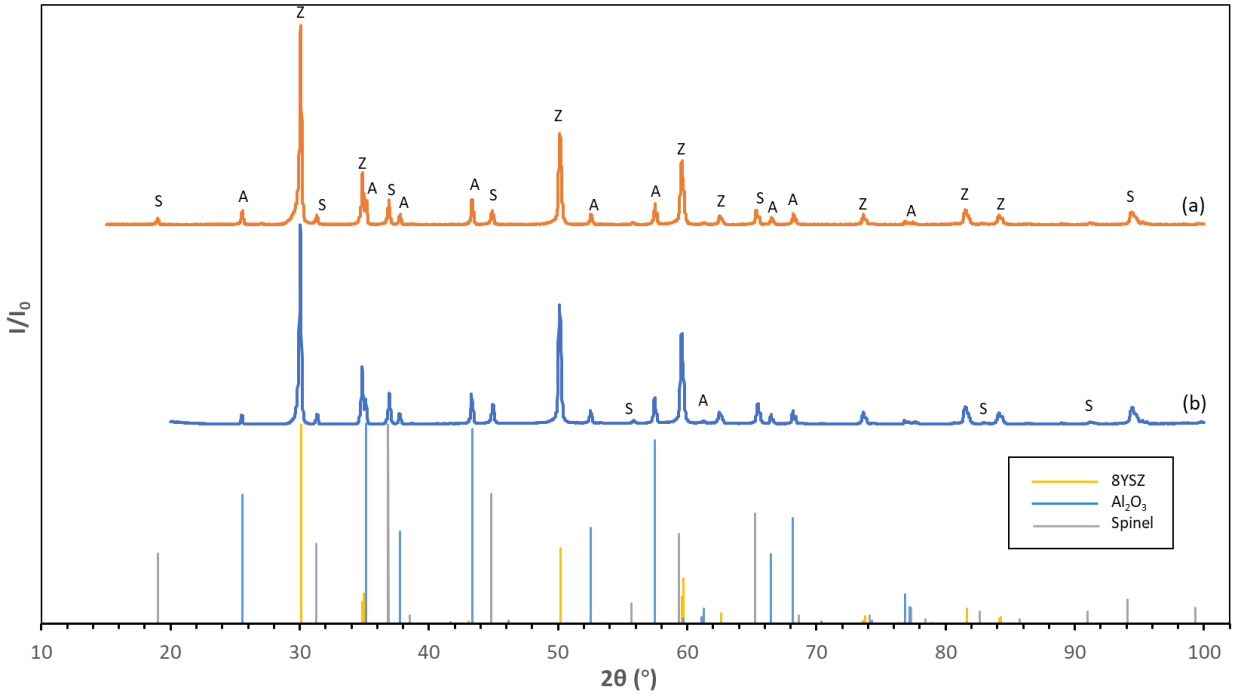

Fig. 4.3 X-ray Diffraction of Sample (a) 3-Phase Fine Grain; (b) 3-Phase Large Grain.

The XRD diagram (See Fig. 4.3) in both large grain and fine grain samples shows correspondence to the standard peak position, no phase change during sintering.

4. Thermal Conductivity Measurements

The samples of interest, measuring conditions and values from *3ω* method are summarized in Table 4.3. Comparison with other literature values and theoretical mixture values are plotted out in Fig 4.4. The thermal measurements were taken at UC Berkeley in the lab of Professor Chris Dames.

Table 4.3 *3ω* Data at Room Temperature and 50℃

	8YSZ	3-P Fine	3-P Large_1	3-P Large_2
23 (℃)	2.27	9.57	11.63	10.52/9.81
50 (℃)	2.24	9.52	14.99	-

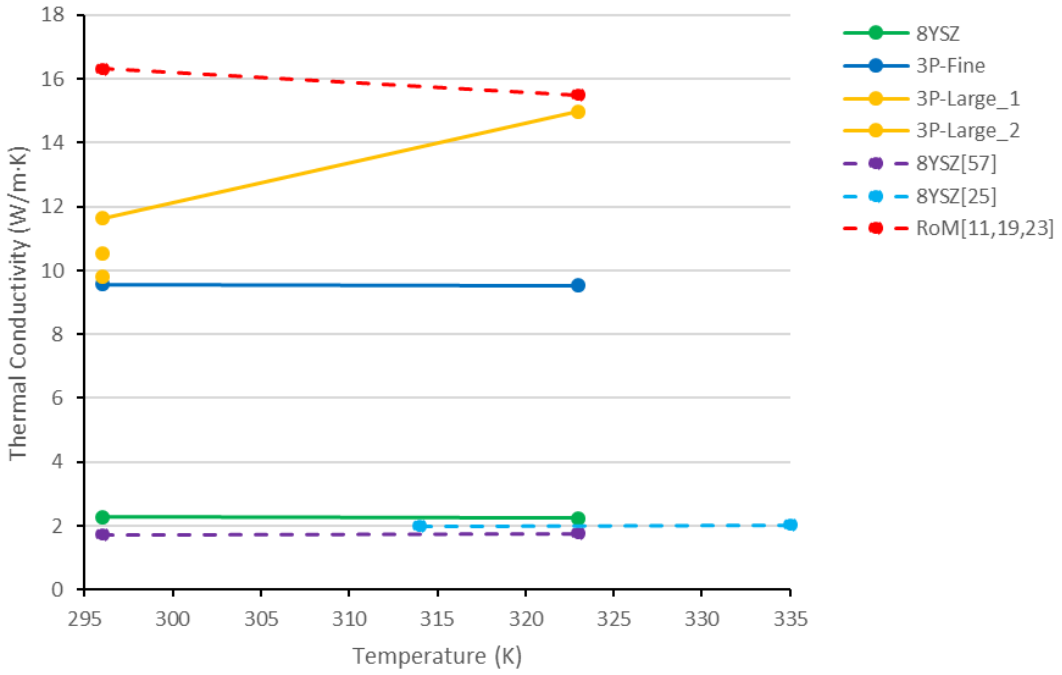

Fig. 4.4 Thermal Conductivity Values from *3ω* Method (Solid lines) and Literature Values (Dash lines)

First, the previous experimental results have two significant drawbacks which are limited measuring temperature range and data sets. However, this current data is in the proper range of thermal conductivity and the trends are the same. The data may deviate slightly due to different samples. Comparing the 8YSZ data with the values from *Angle et al.* [25] by *3ω* method, the values are close, but the *3ω* measurements here are higher, maybe due to different porosity in materials and electrode fabrication. Also, during the data analysis, a calibration parameter was multiplied by the original thermal conductivity. The parameter varies from system to system and it may also vary between different samples. The system we used in UC Berkeley was for biomaterials thermal conductivity measurement, therefore,

for different types of material, calibration based on the system and materials are essential. The 8YSZ thermal conductivity measurements decrease slightly with increasing temperature, but are still within the values from 'benchmark' materials, so are reasonable.

According to the Rule of Mixture (RoM), the thermal conductivity in three equal volume material mixture is 1/3 of the summation of these three. By calculation from the literature values, the ideal thermal conductivity in mixture from room temperature to 50℃ decreases from 16.3 to 15.5 W/m·K. The two types of 3-phase samples are all below this value, but the work of *Angle et al.* [25] already showed that the RoM greatly overestimates the thermal conductivity for multiphases systems. The large grain samples' values are higher than fine grain samples due to the low grain boundary density and porosity in large grain. It should also be noted that measuring two times of second 3-phase large grain sample under room temperature, still gave slightly different values. Data from large grain samples at 50℃ had even higher thermal conductivity than room temperature, which makes it unreliable. For the fine grain samples, the thermal conductivity slightly decreases but no trend can be determined. As is shown Appendix B, the electrodes were not optimized, and flaking of electrodes from surface may have made these measurements less reliable. Al was used for the electrodes as that was supposed to be more stable with temperature, but future work may use gold.

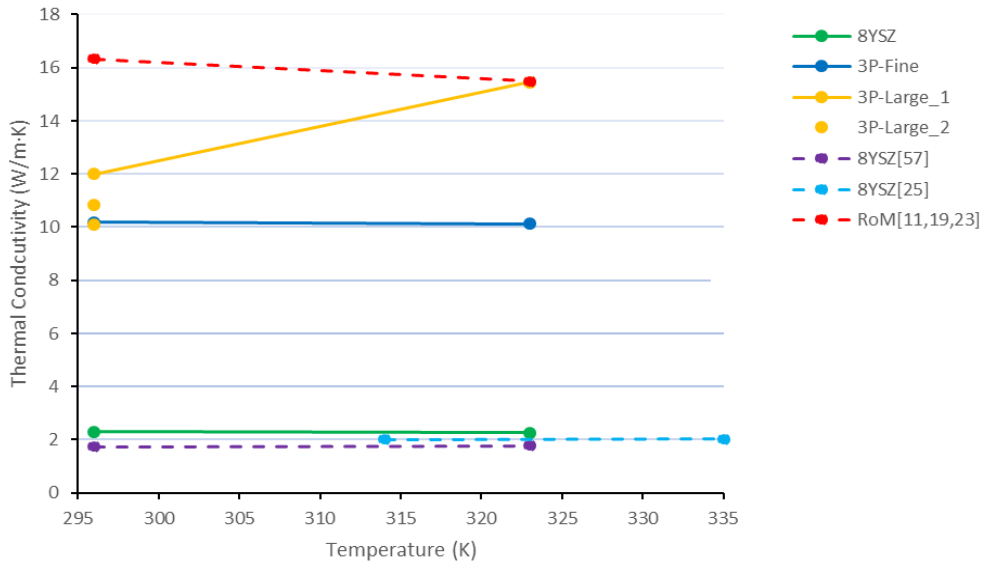

Fig. 4.5 Thermal Conductivity Values from *3ω* Method (Solid lines) with Porosity Correction and Literature Values (Dash lines)

The thermal conductivity values after porosity correction with Eqn 12are higher than experimental values. Due to the low porosity in 8YSZ sample, the values do not change so much. While the fine grain sample relatively changes more and its value is even higher than one of the large grain data point at room temperature. In summary, more data need to be collected on these samples and calibration should to be performed during the system setup.

Thanks for the permission of *Kara Philips* [60], comparison between *3ω* method and Laser flash method (LFM) is accessible. The sample she used was also 3-phase large grain but with started temperature at 90℃. Therefore, by adding a polynomial fitting line we can compare the approximate thermal conductivity at room temperature and 50℃. This method is less accurate due to the thermal property line are inverse relation with temperature. Based on the equation

$$\frac{1}{k} = (A \cdot T) + B \tag{27}$$

Where 1/k is the inverse of thermal conductivity, meaning the overall thermal resistance. T is temperature, A is phonon-phonon scattering (Umklapp scattering), B represents the defects in material. linear fitting results will show the thermal conductivity at room temperature by plug in the value into equation. The thermal conductivity of the 3-phase materials as measured by *3ω* is higher than for the LFM. Further work is required to determine if this is systemic or a problem with the electrodes.

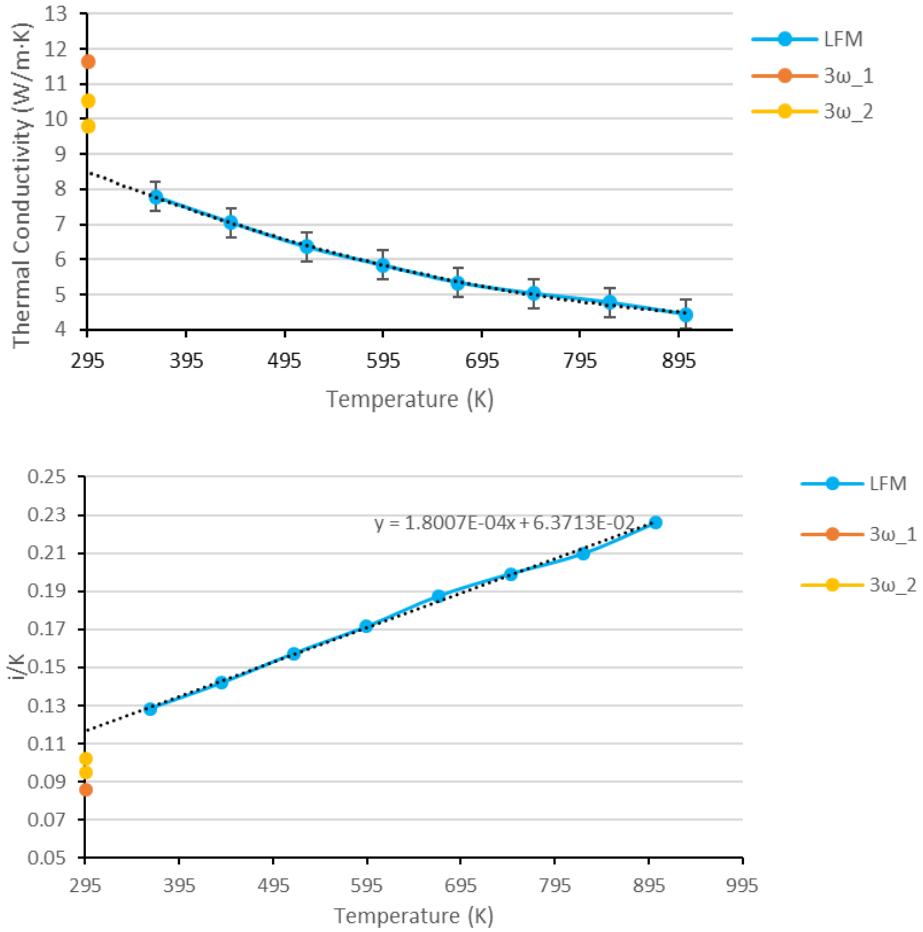

Fig. 4.6 Thermal Conductivity from *3ω* Method and Laser Flash Method (LFM)
(top: polynomial fitting; bottom: linear fitting)

Therefore, the thermal conductivity value at room temperature is 8.54 W/m ·K which is pretty close to the estimate value from polynomial. However, LFM values have

unsatisfactory correspondence to *3ω* outcomes. Future test needs more data from *3ω* method.

To demonstrate a method's reliability, experimental data is compared with modeling results. Thanks for the permission of *Austin Travis* [60], *3ω* data compared with previous OOF2, MOOSE and Bruggeman simulation results are shown in Fig 4.7. Similarly, there were no data points at room temperature and 50℃, therefore, extrapolations help for analysis. Similarly, we also plot out the inverse thermal conductivity in a function of temperature.

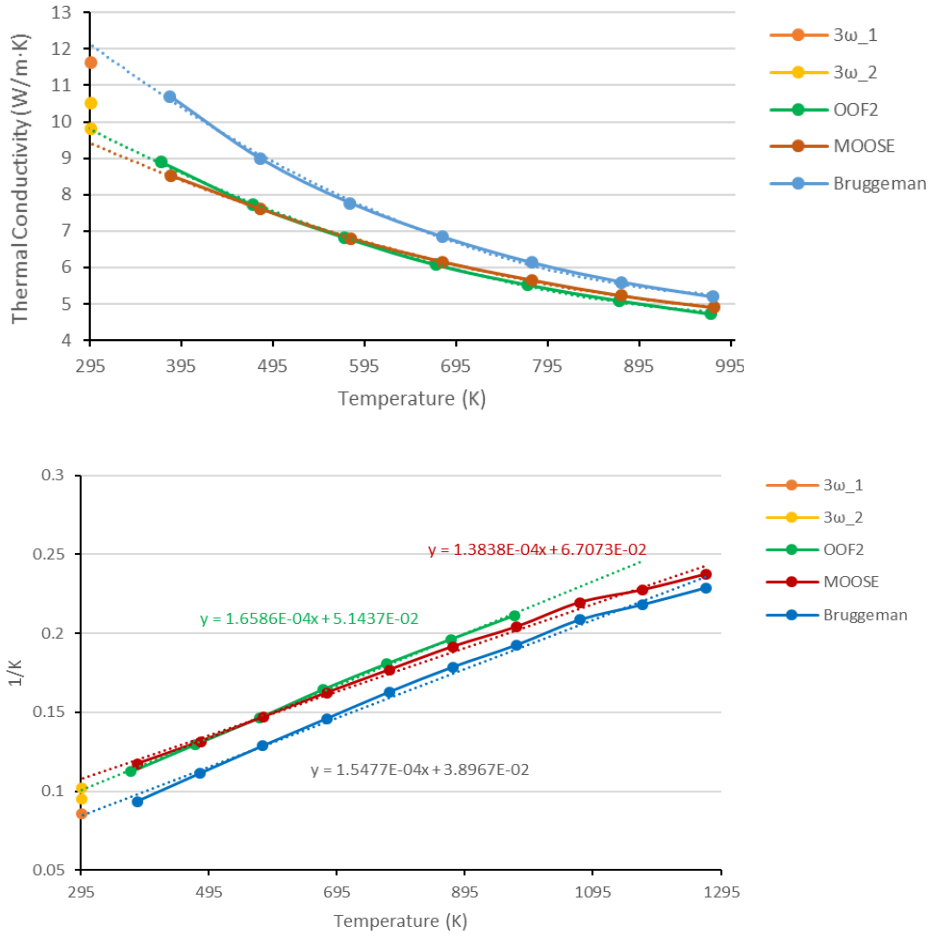

Fig. 4.7 Comparison Between *3ω* Method and Three Simulation Techniques (OOF2, MOOSE, Bruggeman) (top: polynomial fitting; bottom: linear fitting)

Based on the current data, the Bruggeman results deviate from the other two methods. The most promising method among these three is OOF2 which has the same point intersection in both diagrams. Most simulations did not consider grain boundaries and porosity. Usually, simulation results are higher than experimental outcomes. To get better understanding which method more precisely represents the situation, more data should be collected from variable techniques. And for the simulation, multiple defects and factors that may affect thermal conductivity should be concerned. Less deviations happened at higher temperature from the simulation results, which probably due to the inhibition of grain boundaries are more 'transparent' at high temperature.

5. OOF2 Simulation

Colorized SEM images were imported for thermal conductivity simulation (See Fig. 4.8). Due to the random section selection and relative high magnification, the phases in picture shown in Fig. 4.8 are not accurately 1/3-1/3-1/3 distributed. But overall each phase holds an equal volume. Each pixel in the picture represents a phase and assigned thermal conductivity Based on the Eqn. 26 the final averaged thermal conductivity from OOF2 of these specific samples also tested by 3ω was 10.8 W/m· K at room temperature, very close to the value from 3ω method. So the deviation between our results and prior work may be that different microstructures and different amounts of each phase was actually present in our work versus the prior work. It is worth noting that the meshing level and homogeneity of the colorized microstructure have impact on the final values. Future work can be performed directly on Linux or OS system to improve its accuracy.

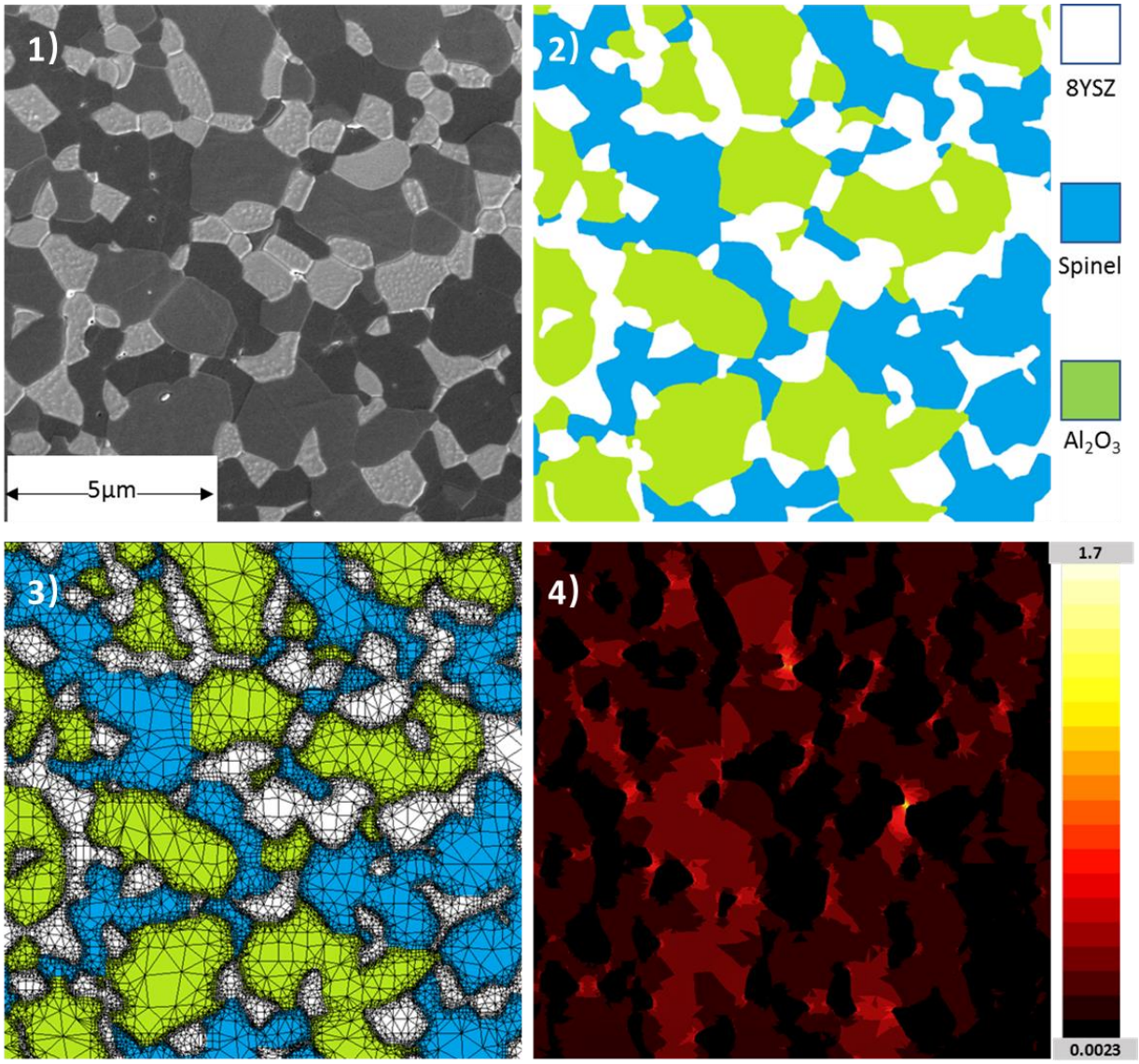

Fig. 4.8 OOF2 Simulation Results 1) SEM SE Image. 2) Colorized Microstructure. 3) Meshed Microstructure 4) Thermal flux simulation result

CONCLUSION AND FUTURE WORK

A *3ω* system was designed in collaboration with Dr. Chris Dames at UC Berkeley and Dr. Bischof at the University of Minnesota. This system is installed and ready to test. Sample preparation, standard operating procedures, and equipment set up are reported in the Appendices. Preliminary results on thermal conductivity from samples at Berkeley show that the different samples had thermal conductivity measurements by *3ω* displaying similar trends to LFM. The 8YSZ samples had the lowest thermal conductivity, and the 3-phase samples had the highest thermal conductivity. The 8YSZ samples were in the approximate range of other reported thermal conductivity data from other researchers. The 3-phase sample had a higher thermal conductivity than measured for another 3-phase sample that supposedly had a similar composition. However, OOF2 computational simulations show that for the microstructure of our 3-phase material, the thermal conductivity is expected to be high than the 3-phase samples used for LFM, and that the thermal conductivity obtained by *3ω* was close to that computationally predicted. Thus, *3ω* appears to be a promising choice for evaluating the relative thermal conductivity new ceramic materials. Future work should include additional sample testing to check for variations between samples and within samples, and better measurements as a function of temperature. Also, future collaborate work with Los Alamos National Laboratory to measure the thermal conductivity of these same samples by LFM should allow for a good comparison between LFM and *3ω* Method. However, the promise of *3ω* measurements has been documented by this research.

REFERENCE

[1] Sims, Ralph EH, Hans-Holger Rogner, and Ken Gregory. "Carbon emission and mitigation cost comparisons between fossil fuel, nuclear and renewable energy resources for electricity generation." *Energy policy* 31.13 (2003): 1315-1326.
[2] Naveh, Alon, et al. "Power and Thermal Management in the Intel Core Duo Processor." *Intel Technology Journal* 10.2 (2006).
[3] Deen, William Murray. "Analysis of transport phenomena." (1998): 433.
[4] https://www.hdiac.org/node/2426
[5] Ormerod, R. Mark. "Solid oxide fuel cells." *Chemical Society Reviews* 32.1 (2003): 17-28.
[6] Stambouli, A. Boudghene, and E. Traversa. "Solid oxide fuel cells (SOFCs): a review of an environmentally clean and efficient source of energy." *Renewable and sustainable energy reviews* 6.5 (2002): 433-455.
[7] Hobbs, Linn W., et al. "Radiation effects in ceramics." *Journal of Nuclear Materials* 216 (1994): 291-321.
[8] Ewing, Rodney C., William J. Weber, and Jie Lian. "Nuclear waste disposal—pyrochlore (A 2 B 2 O 7): Nuclear waste form for the immobilization of plutonium and “minor” actinides." *Journal of Applied Physics* 95.11 (2004): 5949-5971.
[9] Clarke, D. R. "Ceramic materials for the immobilization of nuclear waste."*Annual Review of Materials Science* 13.1 (1983): 191-218.
[10] Yamashita, T., et al. "Irradiation behavior of rock-like oxide fuels." *Journal of nuclear materials* 320.1 (2003): 126-132.
[11] MUNRO, Munro. "Evaluated Material Properties for a Sintered alpha-Alumina." *Journal of the American Ceramic Society* 80.8 (1997): 1919-1928.
[12] Zacheis, George Adam, Kimberly A. Gray, and Prashant V. Kamat. "Radiation-induced catalysis on oxide surfaces: degradation of hexachlorobenzene on γ-irradiated alumina nanoparticles." *The Journal of Physical Chemistry B* 103.12 (1999): 2142-2150.
[13] Pells, G. P. "Radiation effects in ceramic insulators." *MRS Proceedings*. Vol. 373. Cambridge University Press, 1994.
[14] Valdez, James A., et al. "Characterization of an ion irradiation induced phase transformation in monoclinic zirconia." *Nuclear Instruments and Methods in Physics Research Section B: Beam Interactions with Materials and Atoms*218 (2004): 103-110.
[15] Sickafus, Kurt E., et al. "Radiation damage effects in zirconia." *Journal of Nuclear Materials* 274.1 (1999): 66-77.
[16] Thomé, L., et al. "Radiation damage in ion-irradiated yttria-stabilized cubic zirconia single crystals." *The European Physical Journal Applied Physics*24.1 (2003): 37-48.
[17] Navrotsky, Alexandra. "Thermochemical insights into refractory ceramic materials based on oxides with large tetravalent cations." *Journal of Materials Chemistry* 15.19 (2005): 1883-1890.
[18] Ping, Lim Rooi, Abdul-Majeed Azad, and Teng Wan Dung. "Magnesium aluminate (MgAl 2 O 4) spinel produced via self-heat-sustained (SHS) technique." *Materials research bulletin* 36.7 (2001): 1417-1430.
[19] Wilkerson, K. R., et al. "Solid solution effects on the thermal properties in the MgAl2O4–MgGa2O4 system." *Journal of the American Ceramic Society* 96.3 (2013): 859-866.
[20] Sickafus, K. E., et al. "Radiation tolerance of complex oxides." *Science*289.5480 (2000): 748-751.
[21] Sickafus, K. E., et al. "Cation disorder in high dose, neutron-irradiated spinel." *Journal of Nuclear Materials* 219 (1995): 128-134.
[22] Jencic, I. "Radiation damage in nuclear waste materials." (2000).
[23] Schlichting, K. W., N. P. Padture, and P. G. Klemens. "Thermal conductivity of dense and porous yttria-stabilized zirconia." *Journal of materials science*36.12 (2001): 3003-3010.
[24] Carter, C. Barry, and M. Grant Norton. *Ceramic materials: science and engineering*. Springer Science & Business Media, 2007.
[25] Angle, Jesse P., et al. "Comparison of Two-Phase Thermal Conductivity Models with Experiments on Dilute Ceramic Composites." *Journal of the American Ceramic Society* 96.9 (2013): 2935-2942.

[26] Cao, X. Q., R. Vassen, and D. Stoever. "Ceramic materials for thermal barrier coatings." Journal of the European Ceramic Society 24.1 (2004): 1-10.
[27] Giraud, Sophie, and Jérôme Canel. "Young's modulus of some SOFCs materials as a function of temperature." Journal of the European Ceramic Society 28.1 (2008): 77-83.
[28] Petric, Anthony, and Hang Ling. "Electrical conductivity and thermal expansion of spinels at elevated temperatures." Journal of the American Ceramic Society90.5 (2007): 1515-1520..
[29] Tietz, F. "Thermal expansion of SOFC materials." Ionics 5.1 (1999): 129-139.
[30] Carmack, Jon, and Kemal Pasamehmetoglu. Options study documenting the fast reactor fuels innovative design activity. No. INL/EXT--10-19999. Idaho National Laboratory (United States). Funding organisation: DOE-NE (United States), 2010.
[31] Valdez, J. A., et al. "10MeV Au ion irradiation effects in an MgO–HfO 2 ceramic–ceramic (CERCER) composite." Journal of Nuclear Materials 393.1 (2009): 126-133.
[32] Men, Danju, et al. "Radiation damage in multiphase ceramics." Journal of Nuclear Materials 443.1 (2013): 120-127.
[33] Callister, William D., and David G. Rethwisch. Materials science and engineering. Vol. 5. NY: John Wiley & Sons, 2011.
[34] Kittel, Charles. Introduction to solid state physics. Wiley, 2005.
[35] Monachon, Christian, Ludger Weber, and Chris Dames. "Thermal boundary conductance: A materials science perspective." Annual Review of Materials Research 46 (2016): 433-463.
[36] Lee, Jaeho. “Thermal Micro Nano.” University of California, Irvine. Social Science Tower 120, Irvine. 8 Feb. 2017. Lecture.
[37] Bergman, Theodore L., and Frank P. Incropera. *Fundamentals of heat and mass transfer*. John Wiley & Sons, 2011.
[38] Pollack, Gerald L. "Kapitza resistance." *Reviews of Modern Physics* 41.1 (1969): 48.
[39] Swartz, E. T., and R. O. Pohl. "Thermal resistance at interfaces." Applied Physics Letters 51.26 (1987): 2200-2202.
[40] Zeng, Taofang, and Gang Chen. "Phonon heat conduction in thin films: impacts of thermal boundary resistance and internal heat generation."*TRANSACTIONS-AMERICAN SOCIETY OF MECHANICAL ENGINEERS JOURNAL OF HEAT TRANSFER* 123.2 (2001): 340-347.
[41] Wang, Haitao, et al. "Computation of interfacial thermal resistance by phonon diffuse mismatch model." *Materials transactions* 48.9 (2007): 2349-2352.
[42] Zhao, Dongliang, et al. "Measurement Techniques for Thermal Conductivity and Interfacial Thermal Conductance of Bulk and Thin Film Materials." *Journal of Electronic Packaging* 138.4 (2016): 040802.
[43] Maca, K., V. Pouchly, and A. R. Boccaccini. "Sintering densification curve: A practical approach for its construction from dilatometric shrinkage data."*Science of Sintering* 40.2 (2008): 117-122.
[44] Rudtsch, S. "Uncertainty of heat capacity measurements with differential scanning calorimeters." *Thermochimica Acta* 382.1 (2002): 17-25.
[45] Casalegno, Valentina, et al. "Measurement of thermal properties of a ceramic/metal joint by laser flash method." *Journal of Nuclear Materials* 407.2 (2010): 83-87.
[46] Baba, Tetsuya, and Akira Ono. "Improvement of the laser flash method to reduce uncertainty in thermal diffusivity measurements." *Measurement Science and Technology* 12.12 (2001): 2046.
[47] White, Joshua Taylor, et al. "Thermophysical properties of U3Si2 to 1773K."*Journal of Nuclear materials* 464 (2015): 275-280.
[48] Kingery, W. D., et al. "Thermal conductivity: X, data for several pure oxide materials corrected to zero porosity." *Journal of the American Ceramic Society* 37.2 (1954): 107-110.
[49] Marino, G. P. "The porosity correction factor for the thermal conductivity of ceramic fuels." *Journal of Nuclear Materials* 38.2 (1971): 178-190.
[50] Cheaito, Ramez, et al. "Thermal conductivity measurements via time-domain thermoreflectance for the characterization of radiation induced damage."*Journal of Materials Research* 30.9 (2015): 1403-1412.
[51] Cahill et al., "Thermometry and thermal transport in micro/nanoscale solid-state devices and structures." J. of Heat Transfer 124.2 (2002)
[52] Asheghi, M., and Y. Yang. "Micro-and nano-scale diagnostic techniques for thermometry and thermal imaging of microelectronic and data storage devices." *Microscale Diagnostic Techniques*. Springer Berlin Heidelberg, 2005. 155-196.

[53] Cretin, Bernard, et al. "Scanning thermal microscopy." *Microscale and nanoscale heat transfer* (2007): 181-238.
[54] De Koninck, David. "Thermal conductivity measurements using the 3-omega technique: application to power harvesting microsystems." *Masters Abstracts International*. Vol. 48. No. 02. 2008.
[55] Cahill, David G. "Thermal conductivity measurement from 30 to 750 K: the *3ω* method." *Review of* scientific instruments 61.2 (1990): 802-808.
[56] Carslaw, H. S., and J. C. Jaeger. Heat in solids. Vol. 1. Clarendon Press, Oxford, 1959.
[57] Qiu, Lin, et al. "Thermal-conductivity studies of macro-porous polymer-derived SiOC ceramics." International Journal of Thermophysics 35.1 (2014): 76-89.
[58] Dames, Chris. "Measuring the thermal conductivity of thin films: 3 omega and related electrothermal methods." Annual Review of Heat Transfer 16.16 (2013).
[59] Dames, Chris, and Gang Chen. "1 ω, 2 ω, and 3 ω methods for measurements of thermal properties." Review of Scientific Instruments 76.12 (2005): 124902.
[60] Unpublished Work

APPENDIX A

Ceramic Sample Preparation Procedure

1) Wet Milling

For single phase 8YSZ preparation, since raw powder crystallite size is around 30nm, we don't need to mill it. But for 3-phase ceramic powder preparation, we need to use attritor to mill the mixed powder with equal volume in isopropanol and acetone for 12 hours. Use alumina beads as media. This process is helpful in getting fine and uniform particle.

2) Filtering and washing

Prepare a crystallizing dish to collect filtrate. Use a filter to separate medias and suspension, spray isopropanol on top of the beads and wash the suspension remains on beads surface until the filtrate is not so muddy. Then wash milling bowl with isopropanol and pour both liquids into the crystallizing dish.

3) Drying

Put the crystallizing dish on top of a hot plate and set the temperature to 65℃ and keep it for 12 hours. Put a piece of aluminum foil on top of the crystallizing dish to avoid contamination.

4) Grinding

Take out the ceramic chunk and use pestle grind the large pieces to fine powders. The finer this step can get the less time the next step will take.

5) Sieving

Put the powders on the top layer of the sieving machine and put 5 beads on each layer in order to increase the attrition between powders. The powders on the last layer (106 μm) should be collected and put in a glass bottle with lid.

6) Compressing

The mold we used was 12mm in diameter, 15mm deep (See Fig. 1). Pour the powder into a mold and cover with the lid and slightly knock on the table to make sure that the powder is compacted. Then use parafilm to seal the mold tightly and put it inside of a balloon, the balloon should be vacuumized totally. Then put the balloon inside of the Cold Isostatic Press (CIP), make sure it is totally submerged. The compressing pressure should be 55MGPa. Maintain the pressure for 5min then slowly depressurize.

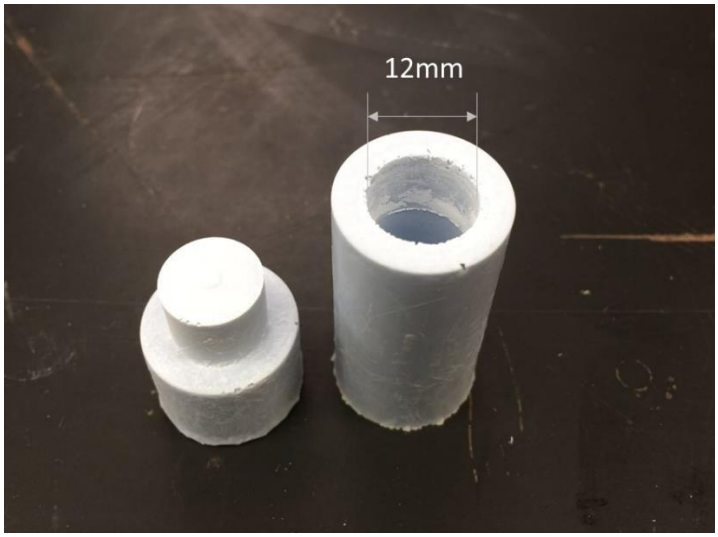

Fig. 1 Photo of a mold for *3ω* method sample preparation

7) Sintering

Take out the ceramic chunk from the mold and measure geometric density using a micrometer. Put some alumina powder as sintering bed then put the sample on top of it, finally add some more powders to fully cover the sample. Using different sintering profile to get various grain size. For 8YSZ single phase and 3-phase large grain sample, ramp the temperature to 1550℃ at a rate of 10℃/min, hold it for 12hrs and ramp down in a speed of 10℃/min. For fine grain, the heating treatment starts from room temperature, then goes up to 1450℃ at a speed of 5℃/min and hold for 0.1hr and ramp down to 1325℃ in

10℃/min. Then hold it for 5hrs and ramp down in 10℃/min to room temperature. The two profiles are shown in Fig. 2.

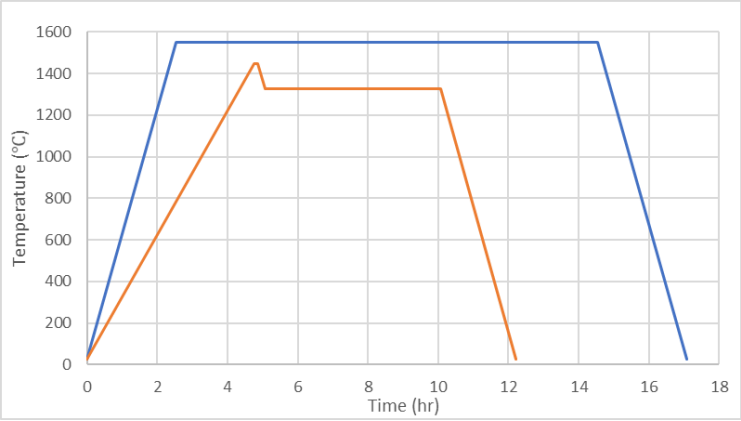

Fig. 2 Heat Treatment Profiles

For orange profile, the 1450℃ plateau is for bonding the grains together and 1325℃ is for grain growth. 5-hour lower temperature dwell makes the average grain size smaller than the single step sintering.

Fig. 3 shows two sintered samples. The common diameter is around 8.2 to 8.9mm and length is around 9.5 to 10.5mm. Values may deviate in the range due to powder density, particle size, distribution, shape, etc.

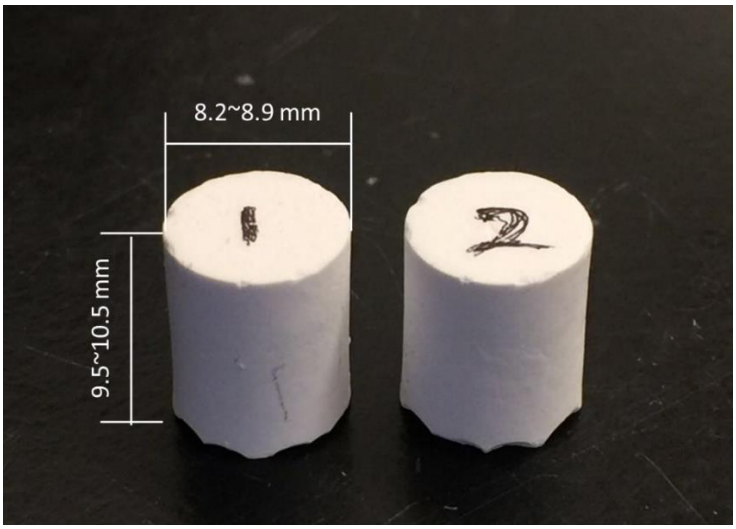

Fig. 3 Two sintered samples

8) Measuring and Calculating

Measure both the geometric density and Archimedes' density in order to get a more accurate density for the samples. Since the diameter varies at a different position, an average value should be obtained after several measurements. In addition, Archimedes' method need to be applied to further approach to the real density. However, the ceramic material is well known for its porous structure. In our study, the 2-step sintering ceramic has more pores near the surface than single step sintering ceramic. In this case, we need to consider using ASTM C20 Method for measuring the density of samples with apparent open pores. Basically, we need to weigh the sample when the opens pores saturated with water. The volume of the sample is the saturated weight minus suspended weight in the water which gives the more accurate density when considering the open pores near surface. However, for our current study, we are looking at the thermal conductivity of the central area of the material, not the near surface region. SEM shows the porous layer only takes up less than 5% of material volume. So before measuring density, we can polish a little bit of the near surface part and then measure the density of the material to get more accurate result. The polishing process can reduce the amounts of open pores near surface.

9) Cutting

Use low speed saw to cut the sample (See Fig. 4 for cutting strategy). For different measurements, the requirement for sample geometry is different. Listed is a table (See Table 1) for both the Laser flash method and the 3ω method sample size requirement.

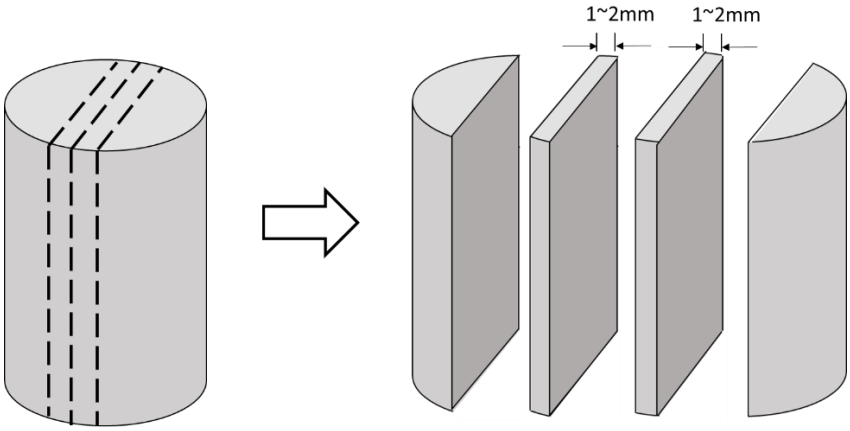

Fig. 4 Schematic Diagram of Cutting Direction

Table 1. LFM and *3ω* Method Sample Geometries

		Length(mm)	Width(mm)	Height/Thickness(mm)	Diameter(mm)
Laser Flash Method	Dilatometry	10	5	5	-
	DSC	-	-	1	6
	LFM	8	8	1	-
3ω Method		8	8	~2	-

10) Polishing

For SEM and *3ω* test, a fine finish sample surface should be complete to get great result. First use SiC abrasive papers to polish the surface of sample in a sequence of 120, 240, 400, 800 grits. Polish with each kind of abrasive paper to see no difference under optical microscope. After that use lapping board with corresponding suspension in a sequence of 6μm, 1μm, 0.1μm and 0.06μm. The final sample surface should not have any black spot or scratch line under optical microscope.

For XRD and Laser flash method test, sample surface only need to be polished a bit to make sure no observable chip or groove on the surface.

11) Postprocessing

For SEM, samples should be etched for 30min at 1200℃ to make the grain boundary more obvious under electron microscopes. Submerge the sample in acetone and sonicate for 5min to remove the particles and contaminations on the surface.

This Appendix does not include detail sample coating for LFM. A graphite layer should be coated before measuring and the thickness of the coating should be controlled to increase accuracy.

APPENDIX B

3ω Sample Evaporation Procedure

Several approaches can achieve similar goals for *3ω* heater line fabrication. Techniques including Thermal Evaporation, E-Beam Evaporation and Sputter Coating. So far, we only tried to perform evaporations on Thermal Evaporator. The mechanism for this technique can be simplified to the metallic evaporation plume deposits on the rotating sample surface.

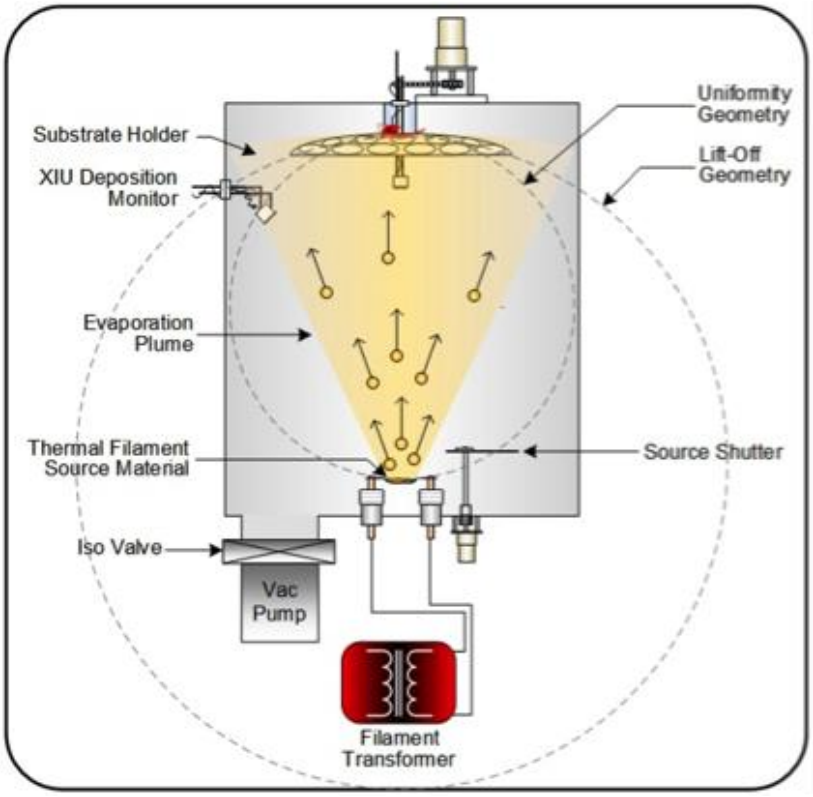

Fig. 1 Schematic Diagram for Thermal Evaporation

The deposition only can be performed when pressure inside is lower than 5×10^{-6} torr. Aluminum is considered to be used because 1) It can be directly applied on the sample surface, no adhesive layer is needed, such as Chromium; 2) Low evaporation temperature; 3) Stable during measuring; 4) Low expense. However, Aluminum is easily to get oxidized

at high-temperature, we need to wait the instrument cool down to room temperature to take samples out.

Based on the previous experience, thermal evaporation in clean room gave a pore quality for the electrode.

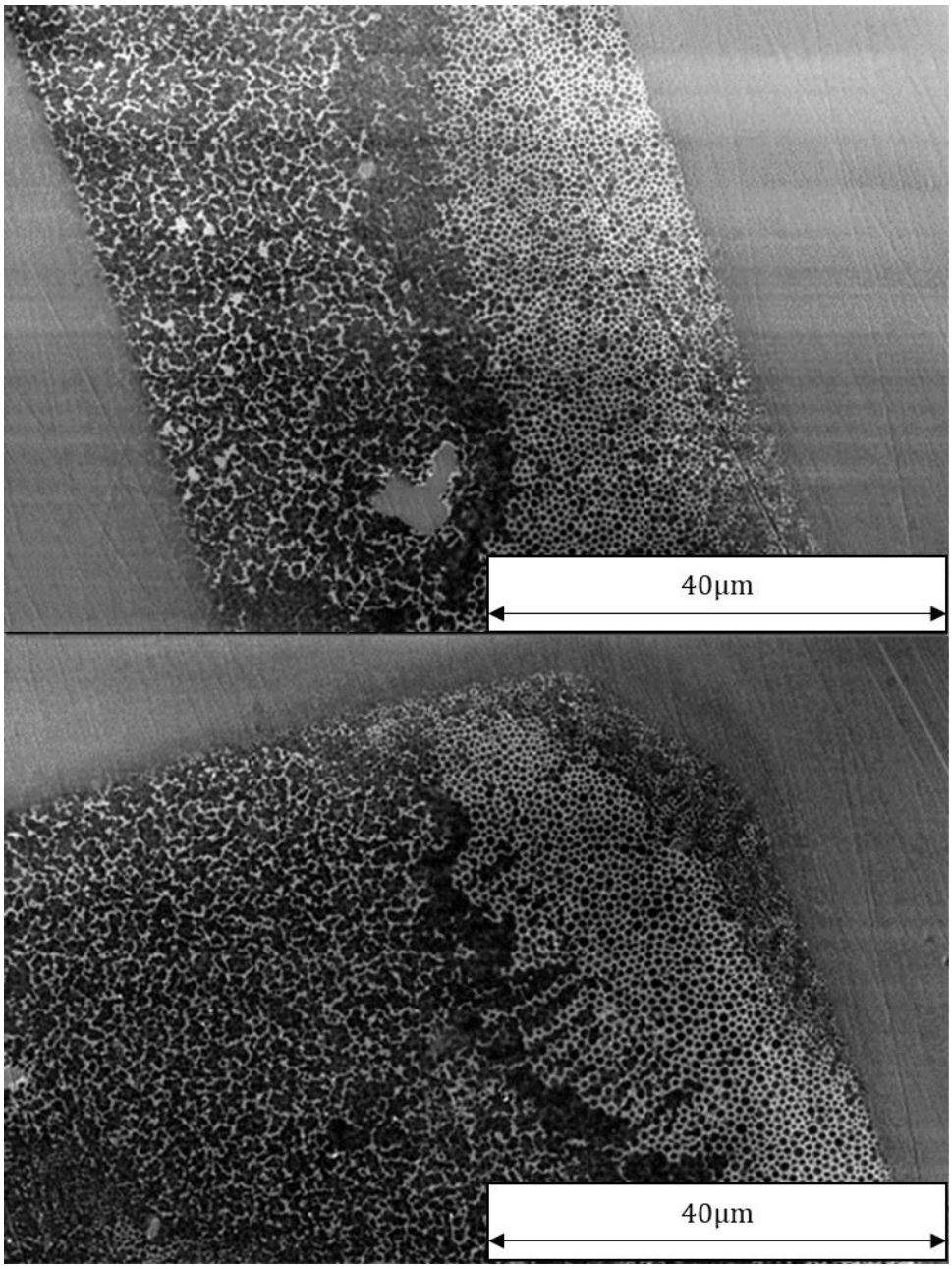

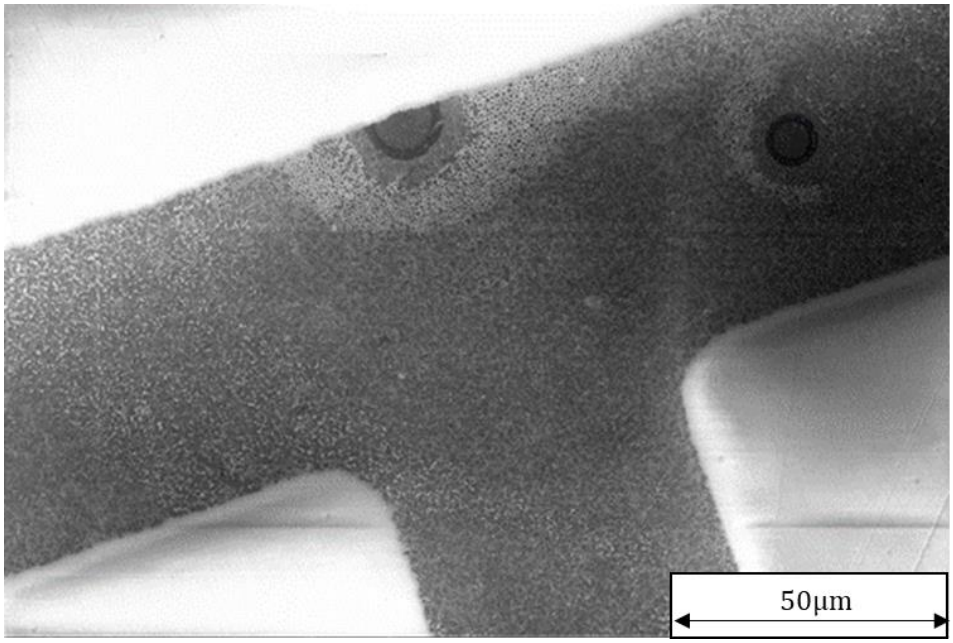

Fig. 2 SEM Image of Thermal Evaporation Results on Sample Surface.

Electron Beam Evaporation (E-beam Evaporation) is another technique but with even wider application with variable materials. The electron gun in the water cooling hearth emits electron beam with extremely high power on to the material that awaits in the crucible. Compare to thermal evaporation, E-beam can control the power density of the electron beam, so both low and high melting temperature materials are applicable in this method. Both evaporations need a quartz crystal deposition control in real time to monitor the rate of deposition, in order to control the thickness of deposition.

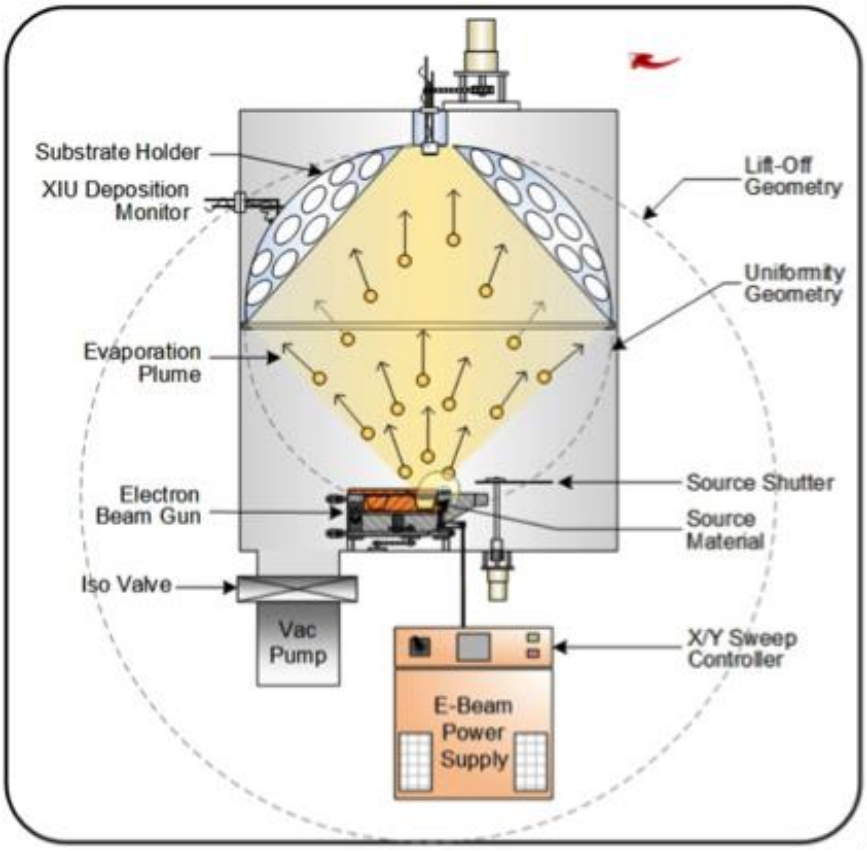

Fig. 3 Schematic Diagram of E-beam Evaporation

Sputter Coating is the method similar to E-beam, instead of electron beam, this instrument uses heavy gas atoms bombarding on the target surface and metal atoms ejected by the ionized gas cross the plasma, deposit onto the sample surface. Advantages for sputter coating is that the sputtered films typically adhere better than evaporated films. Some high melting temperature metals are not restricted by this technique, multiple positions for target and sample are feasible to get same results. The drawbacks for this method are difficulties to control atoms' diffuse transport which make cause the contamination problem for some applications. Layer-by-layer is not achievable in this technique. Depending on the expected results and applications, suitable ways should be selected for performing deposition.

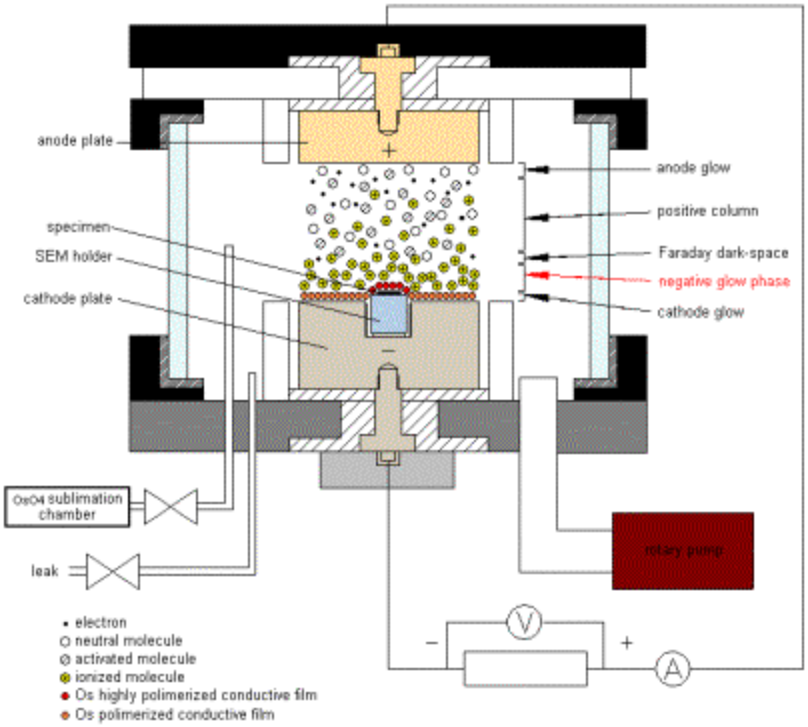

Fig. 4 Schematic Diagram of Sputter Coating

APPENDIX C

3ω Method Operating Procedure

1) Wiring Samples

1. Place a glass slide on a hot plate under optical microscope. Place the sample on a glass slide and put another glass slide with similar thickness of the sample nearby. (to make the wire straight later)
2. Use wire cutter to cut 4 thin straight copper wires with 2 cm long, use sharp end tweezers to place wire directly on all 4 pads, without touching others.
3. Put two epoxies on a glass slide with ratio of 1:1 using the two ends of a toothpick. Use another toothpick to mix them.
4. Prepare another straight copper wire, use sharp end tweezer to make a tiny loop on the one end of the copper wire. Twine the wire on tweezer.
5. Dip the tiny loop in the epoxy mixture and blob on the wire to affix the thin wire to each pad under microscope.
6. Cure epoxy at 150℃ for 15min waiting to see color change.
7. When sample cools down, attach sample to the glass slide with thermal grease.
8. Stick copper tape under each open-end copper wire.
9. Prepare 4 lead wires with exposed interior on each end using wire stripper.
10. Use soldering gun to connect lead wire with thin copper wire on the copper tape.
11. Use Kapton tape to keep sample and copper tape in place if they are moving.
12. Use multimeter to check connection

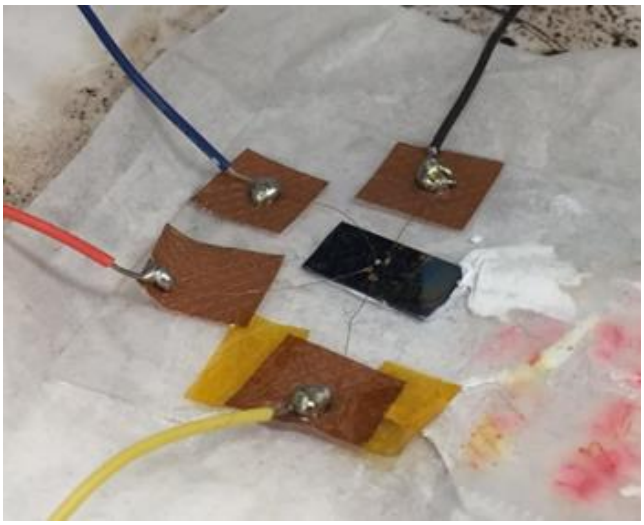

Fig. 1 *3ω* Sample Wiring

2) Electrode Resistance Measurement

1. Use banana plug- gator clip wire to connect four lead wires with a precision multimeter to check resistance. Press Ω4 button to read.
2. Record the temperature with a thermocouple putting on top of the sample.
3. The resistance of the electrode should be below 50 ohms for DSI circuit board.

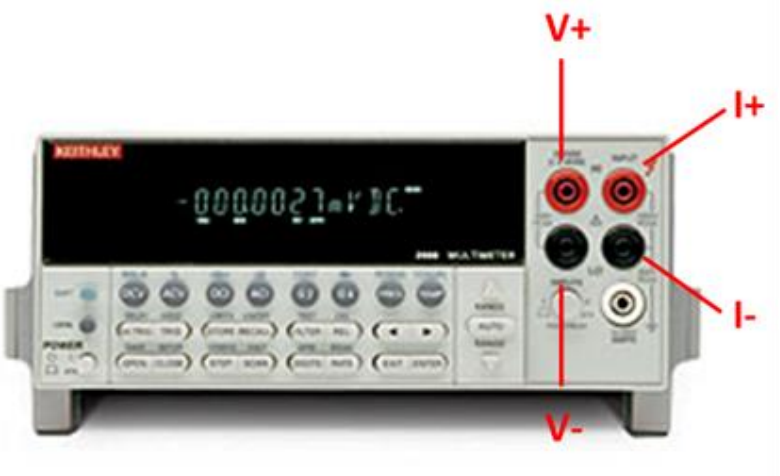

Fig. 2 Keithley Multimeter

3) Thermal Contact Resistance (TCR) Measurement

1. Put the sample with glass slide on a hot plate and put a thermocouple to monitor the temperature of the sample.
2. Use BNC- BNC cables to connect circuit board with Lock-in Amplifier and use BNC-gator clip to connect the sample with circuit board.
3. Measuring under temperature 25℃, 30℃, 35℃, 40℃, 45℃, 50℃

   At each temperature, the input voltages are: 0.004V, 0.008V, 0.012V, 0.016V, 0.020V, 0.024V, 0.028V, 0.032V, 0.036V, 0.040V, 0.050V. Depend on the limit of Lock-in Amplifier, the input voltage range can change to avoid Over Load problem.

R7 | 1009.7

	A	B	C	D	E	F	G	H	I	J	K	L	M
1	Date	Frequency (Hz)	Sensor	Heater Line length (mm)	Heater Line Width (μm)	Heater Line Gold Thickness (nm)	dR/dT	Resistance at T = 0°C (Ohms)	Alpha at T = 0°C (1/°C)	Current Correction Constant	Measurement System	Notes	
2		103		1	50	100	0.13235686	115.137368	0.00114956	0.936	Wyatt 3w		
3													
4		Zero-Current Resistance (Ohms)	118.187			119.154			119.720			120.436	
5		Temperature [C] (from thermocouple reader):	23.0			30.0			35.0			40.2	
6	RMS Lock-in Voltage Output to Circuit (V)	RMS Current Input to Heater Line (mA)	RMS 1w Magnitude Voltage (mV)	RMS Power Dissipatd as Heat (mW)	RMS 1-w magnitude Resistance (Ohm)	RMS 1w Magnitude Voltage (mV)	RMS Power Dissipatd as Heat (mW)	RMS 1-w magnitude Resistance (Ohm)	RMS 1w Magnitude Voltage (mV)	RMS Power Dissipatd as Heat (mW)	RMS 1-w magnitude Resistance (Ohm)	RMS 1w Magnitude Voltage (mV)	RMS Pow Dissipatd Heat (mV
7	0.044	8.2368	981.100	8.081	119.112	987.400	8.133	119.877	993.100	8.180	120.569	997.500	8.216
8	0.04	7.488	890.600	6.669	118.937	896.500	6.713	119.725	901.700	6.752	120.419	905.900	6.783
9	0.036	6.7392	800.500	5.395	118.783	806.000	5.432	119.599	809.500	5.455	120.118	814.500	5.489
10	0.032	5.9904	710.600	4.257	118.623	715.600	4.287	119.458	718.200	4.302	119.892	722.800	4.330
11	0.028	5.2416	621.000	3.255	118.475	625.500	3.279	119.334	628.700	3.295	119.944	632.100	3.313
12	0.024	4.4928	531.800	2.389	118.367	535.800	2.407	119.257	538.600	2.420	119.881	541.600	2.433
13	0.02	3.744	442.900	1.658	118.296	446.400	1.671	119.231	448.700	1.680	119.845	451.200	1.689
14	0.016	2.9952	354.200	1.061	118.256	356.900	1.069	119.157	358.800	1.075	119.792	360.700	1.080
15	0.012	2.2464	265.500	0.596	118.189	267.700	0.601	119.168	268.900	0.604	119.703	270.500	0.608
16	0.008	1.4976	177.060	0.265	118.229	178.540	0.267	119.217	179.320	0.269	119.738	180.420	0.270
17	0.004	0.7488	88.680	0.066	118.429	89.400	0.067	119.391	89.870	0.067	120.019	90.400	0.068
18													

Fig. 3 Spreadsheet Interface

At different voltage (RMS Lock-in Voltage Output to Circuit) read the voltage from Lock-in Amplifier (RMS 1ω Magnitude Voltage). Pay attention to the Zero-Current Resistance in read frame, should be close to the resistance with precision multimeter. Alpha at T=0℃ is the parameter for later calculation.

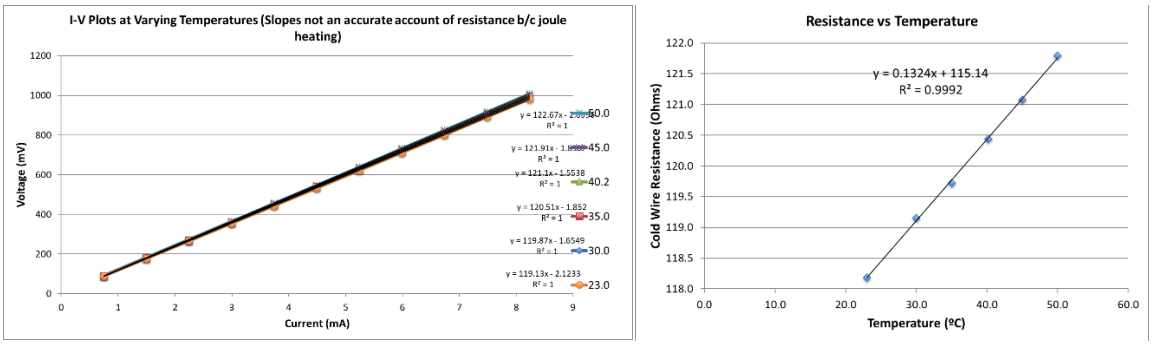

Fig. 4 Linear Fitting of Data

The lines in the left diagram should be straight and R^2 in the right diagram should close to 1, usually higher than 0.9990.

4) Frequency Range Selection

The parameters that involved in frequency calculation are thermal diffusivity, which can also be derived from thermal conductivity, density and heat capacity.

$$\alpha = k / \rho \cdot C \tag{28}$$

α: Thermal diffusivity (m^2/s)

k: Thermal conductivity ($W/m\cdot K$)

ρ: Density under certain temperature (kg/m^3)

C: Heat capacity ($J/K\cdot kg$)

Angular frequency can be derived from the equation which involves thermal diffusivity and thermal penetration depth. Thermal penetration depth usually refers to some range of depth to make sure the heat fluctuation only within that range. Mostly we take the width of the heater line and half of the thickness to get that range.

$$\omega = \alpha / L_P^2$$

ω: Angular frequency (Hz)

α: Thermal diffusivity (m^2/s)

L_P: Thermal penetration depth (m)

5) Performing Thermal Conductivity Measurement

Wire up SR830 Lock-in Amplifier, New Focus 0901 Power Supply, National Instrument 6501 Daq and *3ω* Sample with Circuit Board. Use LabView or Python and change the frequency range to start performing thermal conductivity measurement.

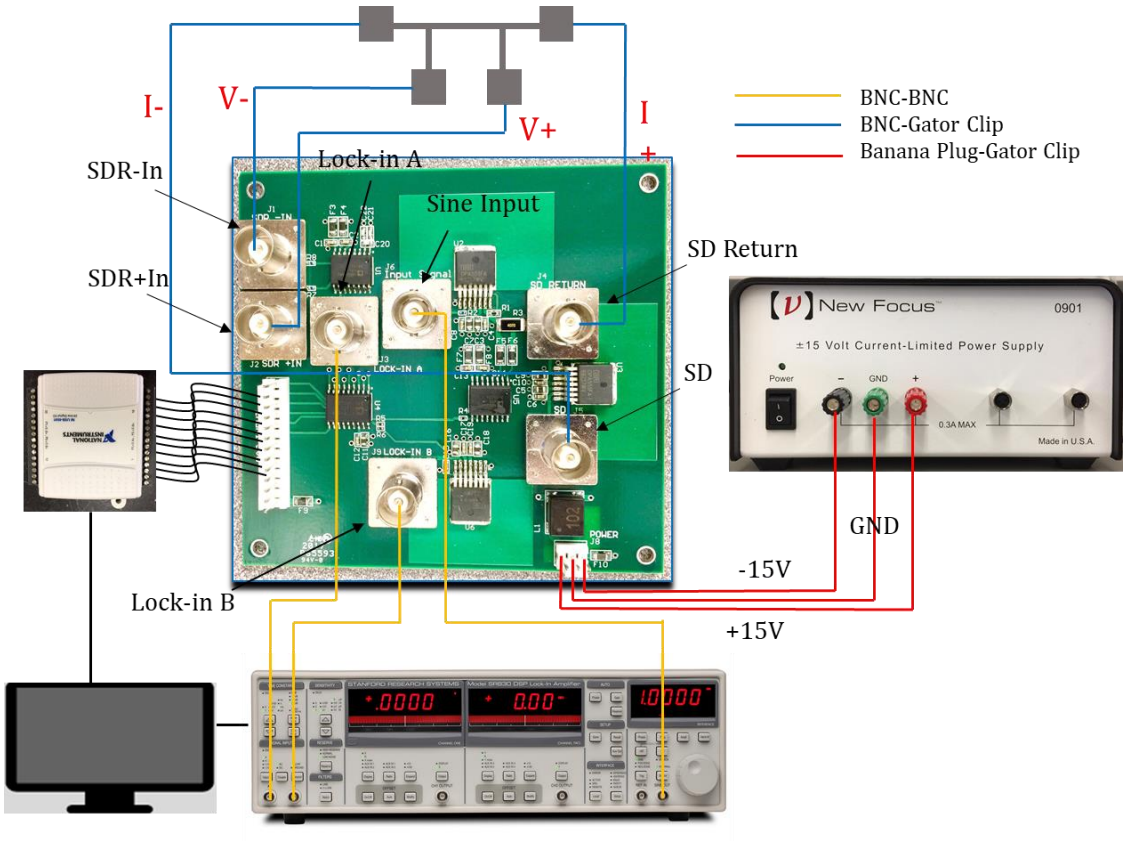

Fig. 5 *3ω* System Wiring Diagram